



A Quantum-Inspired Self-Supervised Network model for automatic segmentation of brain MR images



Debanjan Konar ^{a,c}, Siddhartha Bhattacharyya ^{b,*}, Tapan Kr. Gandhi ^a,
Bijaya Ketan Panigrahi ^a

^a Department of Electrical Engineering, Indian Institute of Technology Delhi, New Delhi, India

^b Department of Computer Science and Engineering, CHRIST (Deemed to be University), Bangalore, India

^c Department of Computer Science and Engineering, Sikkim Manipal Institute of Technology, Sikkim Manipal University, Sikkim, India

ARTICLE INFO

Article history:

Received 28 February 2020

Received in revised form 16 April 2020

Accepted 27 April 2020

Available online 5 May 2020

Keywords:

Quantum computing

Medical image segmentation

Fully Convolutional Neural Network

QIBDS Net

U-Net

ABSTRACT

The classical self-supervised neural network architectures suffer from slow convergence problem and incorporation of quantum computing in classical self-supervised networks is a potential solution towards it. In this article, a fully self-supervised novel quantum-inspired neural network model referred to as Quantum-Inspired Self-Supervised Network (QIS-Net) is proposed and tailored for fully automatic segmentation of brain MR images to obviate the challenges faced by deeply supervised Convolutional Neural Network (CNN) architectures. The proposed QIS-Net architecture is composed of three layers of quantum neuron (input, intermediate and output) expressed as qbits. The intermediate and output layers of the QIS-Net architecture are inter-linked through bi-directional propagation of quantum states, wherein the image pixel intensities (quantum bits) are self-organized in between these two layers without any external supervision or training. Quantum observation allows to obtain the true output once the superimposed quantum states interact with the external environment. The proposed self-supervised quantum-inspired network model has been tailored for and tested on Dynamic Susceptibility Contrast (DSC) brain MR images from Nature data sets for detecting complete tumor and reported promising accuracy and reasonable dice similarity scores in comparison with the unsupervised Fuzzy C-Means clustering, self-trained QIBDS Net, Opti-QIBDS Net, deeply supervised U-Net and Fully Convolutional Neural Networks (FCNNs).

© 2020 Elsevier B.V. All rights reserved.

1. Introduction

The unified concept of quantum information processing explores a new emerging field of research in computer science, referred to as quantum-inspired computing [1–3]. Conventionally, a plethora of quantum-inspired neural networks (QINN) are evolved over the years targeted to solve pattern recognition and classification problems [4–8] using the inherent characteristics offered by quantum mechanics. However, these quantum-inspired neural network models are supervised in nature and rely on complex and time consuming quantum back-propagation algorithms. In addition, the QINN models employ fixed thresholding for the activation function and hence are not applicable for the gray-scale images with wide variation of gray levels.

Magnetic Resonance Imaging (MRI) is a non-invasive technology which allows to acquire and investigate structural images including tumors. The Brain tumor diagnosis essentially requires the key information prevalence to the shape, size, location and

metabolism of brain tumors. However, it is always a daunting task for the radiologists to segment tumor regions and to distinguish various typical brain tumors owing to wide variation in shape, orientation, intensity in-homogeneity and overlapping in the spatial imaging plane. In these circumstances, development of a robust and automated computational technique suitable for MR image segmentation and tumor regions detection received much attention among the computer vision research community. Brain tumor segmentation procedure comprises diagnosing, delineating and isolating tumor tissues from healthy brain tissues.

The primary focus of the suggested work is to propose a new pattern identification integrated self-supervised framework abbreviated as QIS-Net and it is characterized by Quantum-inspired Multi-level Sigmoidal (QMSig) activation function applicable for fully automated segmentation of brain tumors without any external supervision. The proposed QIS-Net architecture relies on a novel quantum-inspired neural model and resorted to self-supervised procedure guided by counter propagation of the network states to obviate complex quantum back-propagation algorithm employed in supervised QINN models. The key thresholding aspect behind the suggested QIS-Net is induced by the spread

* Corresponding author.

E-mail address: dr.siddhartha.bhattacharyya@gmail.com (S. Bhattacharyya).

of intensity in underlying images in an adaptive fashion. Various thresholding schemes have been reported in this article encompassing image context sensitive thresholding in quantum environments. The hyper parameters pertaining to the thresholding process are adaptive in nature and depend on image pixel intensity. It may be noted that the proposed quantum-inspired self-supervised architecture is implemented on a classical computer relying on quantum neuron models and procedures [4,8–10] and hence the suggested model architecture is referred to as quantum-inspired self-supervised neural network (QIS-Net) instead of quantum self-supervised neural network architecture. The major contributions of the manuscript are as follows.

1. In this work, the standard bi-level sigmoidal activation function employed in our previous work (QBDSOONN architecture) [9,10] has been extended to a novel Quantum Inspired Multi-level Sigmoid activation (QMSig) function to address the gray level heterogeneity pertaining to images.
2. Our self-supervised QIS-Net resorts to a functional modification instead of replicating the identical network architecture for each gray level by introducing a novel quantum-inspired network model characterized by a quantum-inspired multi-level sigmoidal activation function (QMSig) thereby cutting down both space and time complexities.
3. The suggested quantum-inspired self-supervised neural network model embedded in the QIS-Net architecture relies on invoking imaginary section of the quantum information processing which is the major distinction with the QIBDS Net [11] for Brain MR image segmentation. Hence, the present attempt tries to explore the inherent quantum correlations thereby yielding faster convergence of the network architecture.
4. The incorporation of quantum computing provides better convergence of the proposed QIS-Net architecture by means of incorporating the frequency components of the interconnection weights and the network inputs thereby enabling faster convergence of the network states in addition to fast and accurate MR image segmentation outcome.

The suggested QIS-Net architecture is applicable for any gray scale image segmentation and the outcome is subject to investigation. However, in this paper, the hyper-parameters of current network architecture are tailored solely for the application of brain MR image segmentation. Rigorous experiments have been carried out on large Nature data sets of T_1CE images [12].

The remaining portion of the report is organized as follows: an in-depth review of the relevant methods for brain MR image segmentation has been discussed in Section 2. This section also elucidates the focus area of research with motivation. The basic concepts of quantum computing are illustrated in Section 3. A short description about the suggested QIS-Net architecture with novel quantum-inspired neural model and Quantum-inspired Multi-level Sigmoidal (QMSig) activation function has been elaborated in Section 4. Section 5 sheds light MR image segmentation using the proposed quantum-inspired self-supervised architecture. Results and discussions are reflected in Section 6. Finally, remarks about conclusion and future work are presented in Section 7.

2. Literature review

Artificial Neural Networks (ANN) based frameworks for MR image segmentation received great attention owing to their parallel and adaptive computing capabilities [13,14]. Notable examples include the fuzzy logic inspired ANN for MR image segmentation [15–17]. Kumar et al. introduced a multi-class Artificial Neural Network (ANN) classifier applied to T_1C MR images segmentation with dimensionality reduction through Principal Component

Analysis (PCA) [14]. A Self-Organizing Feature Map (SOFM) based MR image segmentation by Ortiz et al. [18] deserves special mention due to its self-organizing capability. However, the aforementioned ANN inspired approaches explicitly rely on intensity and feature information to obtain anatomically accurate segmentation of MR images. Recent proposals investigate the use of Convolutional Neural Networks (CNNs) [19,20] to avoid enormous amount of redundant information and features in brain tumor segmentation and have gained popularity among the researchers. Zikic et al. [21] employed a shallow CNN with two convolution layers separated by max-pooling with stride 3, followed by one fully-connected (FC) layer and a soft max layer. Lyksborg et al. [22] suggested a binary CNN to identify the complete tumor. Recently, an automatic MR image segmentation method based on Convolutional Neural Networks (CNN) [19] is proposed exploring small 3×3 kernels in order to minimize the effect of over fitting during training. In addition, U-Net [23] architecture has gained much popularity in 2D slice MR image segmentation. However, in contrast to automated segmentation and brain tumor region detection, CNNs require large amount of manually annotated images for accurate feature learning and extensive pre-processing, which is expensive to acquire and suffers from lack of expert image analysis. Hence, self-supervised/semi-supervised/weakly supervised procedures have received much attention in recent years in the field of medical image segmentation [24,25]. However, these networks are not fully self-supervised and rely on pre-trained 3D neural network models.

Quantum-inspired artificial neural network is evolving due to the conglomeration of inherent parallelism, inference and entanglement offered by quantum computation. Quantum neural network is a quantum replica of classical network architecture which is ruminatively proposed by S. Kak [26]. A multi-level quantum neural network model is suggested by Purushothaman et al. [27] relying on the principle of superposition. Of late, Kouda and Matusi et al. [6,7] introduced a single layer quantum Perceptron model. Recently, Grover quantum learning algorithm guided single hidden layer hybrid quantum neural network deserves special mention [28]. Li et al. [29] proposed a quantum-inspired neural network incorporating controlled-Hadamard gates. Lately, Matusi et al. [30] introduced single and two *qbit* rotation gate. Konar et al. [9,10] also employed single *qbit* rotation gate in the network model architecture. The quantum-inspired neural network models take recourse to quantum entanglement properties of quantum computing and therein associates the input and output patterns in the suggested network architecture [31]. Often, in QINN models, the quantum neural computing is based on the real values and the potential of quantum entanglement is not fully exploited [32]. The same is applicable to quantum gate operations which enable to shift the phase of real angle. However, the quantum bit or *qbit* is a bi-level quantum state in complex Hilbert space.

A fast and efficient binary image segmentation is contributed by Bhattacharyya et al. [5] which mimics the multi-layer self organizing neural network (MLSONN) [33] architecture in the quantum environment. The quantum back-propagation algorithm is introduced in the proposed quantum multi-layer neural network (QMLSONN) architecture tailoring interconnection weights (represented as rotation gates) and it is reported that the QMLSONN architecture outperforms the classical MLSONN [33] architecture. In order to obviate the complex inherent time consuming quantum back-propagation algorithm, Konar et al. [9,10] recently suggested a quantum-inspired self-supervised network architecture referred to as the Quantum Bi-directional Self-Organizing Neural Network (QBDSOONN) architecture relying on the real valued quantum neural computing with bi-level sigmoidal activation function suitable for binary image segmentation. The QBDSOONN

architecture exhibits through counter propagation of the network states instead of the time intensive quantum back propagation algorithm used in QMLSONN. Recently, Konar et al. [11] has proposed a Quantum-Inspired Bi-Directional Self-supervised Neural Network (QIBDS Net) for Brain MR image segmentation rely on the computation of the real part of *qbits* and achieved promising outcome. The optimized version of the same network architecture referred to as Quantum-Inspired Optimized Bi-Directional Self-supervised Neural Network (Opti-QIBDS Net) [34] is also contributed for the same purpose and obtained optimal outcome compared to QIBDS Net. It is also worth noting that Ghosh et al. [35] also proposed a self-organizing classical neural network for gray scale image segmentation by replicating the identical network architecture for each gray scale resulting in greater complexity. In this article, automated segmentation of brain images is accomplished using QIS-Net architecture characterized by quantum-inspired neural network model and QMSig activation function with minimum human intervention and finding tumor regions without external supervision or training.

2.1. Motivation

Deep learning framework based automatic medical image segmentation often falls short in accuracy for unseen medical image classes and robustness owing to the following inherent challenges.

1. There is a requirement of labeled training set of medical images to train a CNN suitably. Due to lack of medical image analysts and expensive expert annotation, the related lesions are not sufficiently available in the data sets.
2. The requirements of high computational (GPU) and memory resources for the extensive training of deep learning frameworks are expensive and time consuming.
3. In automatic MR image segmentation, CNN architectures often suffer from over fitting and slow convergence problems and hence huge efforts are required for appropriate tuning of the hyper parameters of the underlying architecture.
4. In addition, CNN based medical image segmentation also suffers due to lack of image specific adaptability.

A promising alternative to deeply supervised convolutional neural network architecture is the self-supervised or self-organized neural network architecture without any external supervision or training. The novel quantum-inspired self-supervised neural network model is a formidable contribution in this new horizon of research and presented in this article. Moreover, the assimilation of quantum information processing with the QIS-Net quantum neuron model architecture explores the Hilbert space invoking imaginary section of the *qbits* and quantum gates (which are not felicitated in QBDSONN architecture [9,10]) and offers faster convergence. This fast convergence of the suggested network architecture yields precise and time efficient segmentation in real-time owing to the fact that lesser number of false positive and false negative pixels lead to high dice similarity which is always desirable in tumor segmentation on medial images rather than accuracy and hence serves as the inspiration behind incorporation of quantum computing in the current quantum neural network architecture model.

3. Fundamentals of quantum computing

The basic principles of quantum mechanics offer to create computational devices capable of implementing quantum computing algorithms. Quantum mechanical operations like superposition, coherence, decoherence, entanglement [36] are employed to characterize the basic states of quantum computing and it is referred to as *qbits* or quantum bits.

3.1. Concept of *qbits*

A quantum bit or *qbit* [37] is the constituent unit of processing in quantum computing. Unlike a classical bit, a *qbit* resides in a Hilbert space with superposition of eigenstates $|0\rangle$ and $|1\rangle$. Any *qbit* state can be written from the principle of superposition as:

$$|\psi\rangle = \beta_0|0\rangle + \beta_1|1\rangle = \begin{bmatrix} \beta_0 \\ \beta_1 \end{bmatrix} \quad (1)$$

where, β_0 and β_1 are complex numbers and satisfy the normalization criterion

$$|\beta_0|^2 + |\beta_1|^2 = 1 \quad (2)$$

$|\beta_0|^2$ and $|\beta_1|^2$ are probabilities for occurrence of eigen states $|0\rangle$ and $|1\rangle$ in a quantum state respectively.

The Hilbert space comprises a set of superimposed quantum states $|\phi_j\rangle$ containing 0 – 1 and describes the quantum system using the wave function ψ [38].

$$|\psi\rangle = \sum_j^n p_j|\phi_j\rangle \quad (3)$$

where the basic states $|\phi_j\rangle$ are coherently defined in the Hilbert space. $|p_j|^2$ is obtained through quantum observation of the coherent states $|\psi\rangle$ and p_j is a complex number. A real physical system can be depicted as wave function ψ and it must collapse [39] to exactly one of the basic state either 0 or 1, subjected to the condition that the sum of the probabilities $|p_j|$ is unity.

$$\sum_j^n |p_j|^2 = 1 \quad (4)$$

The wave function $|\psi\rangle$ governs a coherent quantum system containing superposition of basic states $|0\rangle$ and $|1\rangle$, which interact with the real physical system on measurement.

The probability for quantum state $|\psi\rangle$ is being observed using Dirac notation and computed as $|\langle\phi|\psi\rangle|^2$. An eigen state $|\psi_j\rangle$ comprising $|0\rangle$ and $|1\rangle$ can be stated as:

$$|\phi\rangle = \frac{2}{\sqrt{5}}|0\rangle + \frac{1}{\sqrt{5}}|1\rangle \quad (5)$$

Unlike classical bits, the coherent quantum state $|\phi\rangle$ exists in superposition of the eigen state $|0\rangle$ and $|1\rangle$. Therein, the probability of $|1\rangle$ measured in eigen states $|\phi\rangle$ is evaluated using Born rule as:

$$|\langle 1|\psi\rangle|^2 = \frac{1}{5} \quad (6)$$

Identically, the probability of $|0\rangle$ measured in eigen state $|\phi\rangle$ is $\frac{4}{5}$.

3.2. Quantum logic gates

Quantum algorithms applicable on single or small number of *qbits* are expressed as quantum logic gates and are reversible in nature. Examples include the phase-shift gate which is defined as follows [8].

$$f(\alpha_1 + \alpha_2) = f(\alpha_1)f(\alpha_2) \quad (7)$$

where $f(\alpha) = e^{i\alpha} = \cos \alpha + i \sin \alpha$ and i is an imaginary unit. The phase reverse operator or the controlled NOT gate is defined as

$$f\left(\frac{\pi}{2}\gamma - \alpha\right) = \begin{cases} \sin \alpha + i \cos \alpha & (\gamma = 1) \\ \cos \alpha - i \sin \alpha & (\gamma = 0) \end{cases} \quad (8)$$

The single *qbit* rotation gate is a phase shift gate defined as

$$R(\alpha) = \begin{bmatrix} \cos \alpha & -\sin \alpha \\ \sin \alpha & \cos \alpha \end{bmatrix} \quad (9)$$

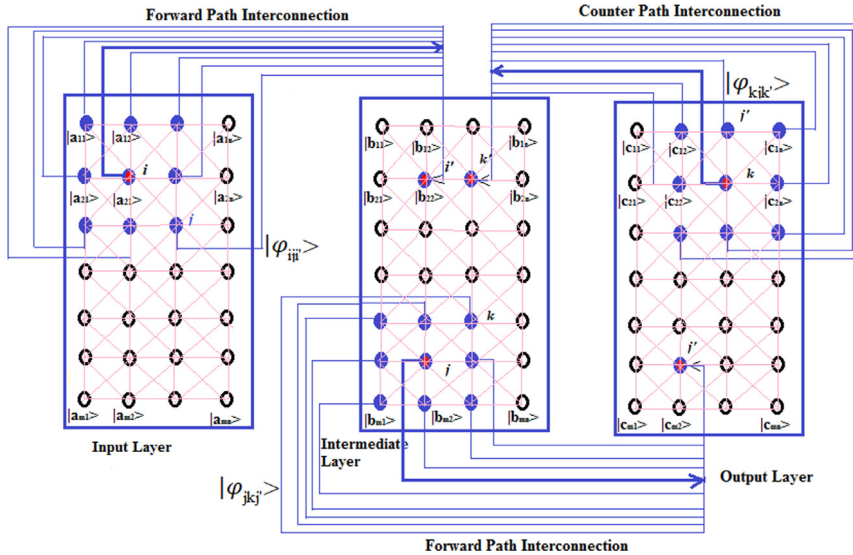


Fig. 1. Quantum-Inspired Self-Supervised Network (QIS-Net) architecture (Few Inter-layer connections are provided for visibility).

The transformation of a single *qbit* is performed as follows:

$$\begin{bmatrix} \beta'_0 \\ \beta'_1 \end{bmatrix} = \begin{bmatrix} \cos \alpha & -\sin \alpha \\ \sin \alpha & \cos \alpha \end{bmatrix} \times \begin{bmatrix} \beta_0 \\ \beta_1 \end{bmatrix} \quad (10)$$

Quantum logic gates (Rotation gate and control NOT gate) are reversible in nature unlike various classical gates and are implemented using unitary representation fulfilling the essence of quantum computation. In the superimposed Hilbert Space, the *qbits* are operated using linear unitary operations.

3.3. Quantum-inspired neural network (QINN)

A multi-layer quantum inspired neural network is constituted of quantum neurons in a layered architecture [9,10]. The network input of *j*th sample neuron, x_j is transformed in to quantum state $[0, \pi/2]$ as

$$z_j = f((\pi/2)\sigma_{qinn}(x_j)) \quad (11)$$

where $\sigma_{qinn}(x)$ is the standard sigmoid activation function defined in the range $[0, 1]$ with x as an input as

$$\sigma_{qinn}(x) = \frac{1}{1 + e^{-x}} \quad (12)$$

Considering a QINN with multiple inputs, single output and characterized by quantum gates, the input-output relation of a basic quantum neuron in the *t*th iteration at hidden and output layers comprising *m* neurons can be modeled as [8]

$$z_j^t = f(h_j^t) \quad (13)$$

$$h_j^t = \frac{\pi}{2}\delta_j^t - \arg(u_j^t) \quad (14)$$

here,

$$u_j^t = \sum_k^m f(\omega_{k,j}^t) f(z_k^{t-1}) - f(\xi_j^t) \quad (15)$$

where $\omega_{k,j}$ denotes the quantum phase transformation parameters in between the input neuron *k* to output neuron *j* and ξ_j^t is the threshold parameter. δ_j represents the quantum rotation parameter.

The output of *i*th quantum neuron at the output layer (denoted as z_i^{0u}) of QINN is obtained using quantum observation, considering the probability of state $|1\rangle$ as defined by

$$u_{qinn_i} = |\text{Im}(z_i^{0u})|^2 \quad (16)$$

where, $\text{Im}(z_i^{0u})$ refers to the imaginary part of z_i^{0u} .

4. Quantum-inspired self-supervised network (QIS-Net) architecture

The QIS-Net architecture is composed of trinity layers of quantum neurons and arranged as input, hidden and output layers described *qbits*. A simplified diagram of QIS-Net architecture is illustrated in Fig. 1.

The input layer of the QIS-Net architecture acts as a gateway and transfers normalized image information to the successive intermediate and output layers for further processing. The image pixels are fed to the input layer as quantum bits and propagates from the input to intermediate layer for subsequent processing. All the three layer of quantum neurons are constituted as *qbits* using the following matrix notation.

$$\begin{bmatrix} |\psi_{11}\rangle & |\psi_{12}\rangle & |\psi_{13}\rangle & \dots & |\psi_{1m}\rangle \\ \dots & \dots & \dots & \dots & \dots \\ \dots & \dots & \dots & \dots & \dots \\ \dots & \dots & \dots & \dots & \dots \\ |\psi_{n1}\rangle & |\psi_{n2}\rangle & |\psi_{n3}\rangle & \dots & |\psi_{nm}\rangle \end{bmatrix}$$

Here, $|\psi_{ij}\rangle$ depicts a *qbit*. The proposed QIS-Net architecture offers fully connected trinity layers of neurons described by *qbits*. The intra-connection weights among the intra-connected neurons in each layer are set to $\frac{\pi}{2}$ (Quantum state). The input layer is organized with the *qbit* information of 8-connected neighborhood subsets of each seed neuron and accumulated at the central neuron of the intermediate layer through interconnections. The output layer is also connected with the intermediate layer in same fashion and quantum states are propagated in forward direction from input to output through the intermediate layer. Consequently, the intermediate output states are also fed to the hidden layer from the output layer for further processing via counter-propagation.

Two fold schemes have been adapted by the proposed QIS-Net architecture incorporating the pixel information and the interconnection weights are represented by *qbits* and updated using

rotation gates. The rotation angle of each quantum gate is determined by the relative quantum fuzzy measures of the pixel intensity at the constituent quantum neurons between the layers. These two key features in the suggested network parameters: the angle of rotation for updating interconnection strength and threshold are as α and γ respectively. The inter-connection strengths, $\varphi_{ijj'}$ in between two adjacent layers of the proposed QIS-Net architecture are set to the relative measures of quantum fuzzy membership grades at the corresponding neuron of the adjacent layer as follows:

$$|\varphi_{ijj'}\rangle = \begin{bmatrix} \cos\alpha_{i,j} \\ \sin\alpha_{i,j} \end{bmatrix} \quad (17)$$

The relative measure of quantum fuzzy membership grades enables to detect the edges between foreground and background pixels.

$$\alpha_{i,j} = \frac{\pi}{2} - (\mu_i - \mu_{i,j}); j \in \{1, 2, 3, \dots, 8\} \quad (18)$$

where, pixel intensity of the i th quantum seed neuron is μ_i and one of its 8-connected neighborhood is $\mu_{i,j}$. The sum of intensities (denoted by x'_i) for all the 8-connected neighborhood pixels of every seed pixel is propagated to the corresponding seed neuron of the subsequent layer as follows:

$$x'_i = \sum_j \varphi_{ijj'} \mu_{i,j} \quad (19)$$

Quantum fuzzy context sensitive activation (denoted as ξ_i) of a seed neuron i is being measured as the contribution of second order (8-connected) neighborhood based image pixel intensities as follows:

$$|\xi_i\rangle = \begin{bmatrix} \cos\gamma_i \\ \sin\gamma_i \end{bmatrix} \quad (20)$$

$$\gamma_i = 2\pi \times \left(\sum_j \mu_{i,j} \right) \quad (21)$$

Quantum fuzzy context sensitive thresholding enables the forward and counter propagation of information. The bi-directional propagation of the quantum states between the intermediate and output layers through self-organizing the inter-connection weights, is the basis of networks dynamics of QIS-Net architecture. The suggested quantum neural model incorporated in the QIS-Net presented in the following subsection.

4.1. Quantum-inspired self-supervised neural network model

The basic input-output relation of a j th basic quantum neuron in the t th sample sets at network layer of the suggested model is defined as follows:

$$|z_j^t\rangle = \sigma_{QJS-Net}(\sum_k^{n \times m} f(z_j^{t-1}) \langle \varphi_k^t | \xi_k^t \rangle) \quad (22)$$

i.e.,

$$\begin{aligned} |z_j^t\rangle &= f\left(\frac{\pi}{2} \delta_j^t - \arg\left\{\sum_k^{n \times m} f(\omega_{k,j}^t) f(z_j^{t-1}) - f(\xi_j^t)\right\}\right) \\ &= \sigma_{QJS-Net}\left(\sum_k^{n \times m} f(z_j^{t-1}) \{ \cos((\omega_{k,j}^t) - v_j^t) + i \sin((\omega_{k,j}^t) - v_j^t) \}\right) \end{aligned} \quad (23)$$

where, z_j depicts the output of the quantum neuron j , $\omega_{k,j}^t$ denotes the quantum phase transformation parameters between the input neuron k to hidden neuron j and ξ_j^t is the threshold parameter. The parameters associated with rotation and the control NOT gate

are denoted as δ_j^t , the activation and the inter-connection link are designated as v_j and $|\varphi\rangle$ respectively. Here, i is an imaginary number, $\sigma_{QJS-Net}$ is QMSig activation function and discussed in the following Section 4.2. True outcome ($|1\rangle$) is obtained on from j th quantum neuron on observation as

$$y_j^t = |\text{Im}(z_j^t)|^2 \quad (24)$$

i.e

$$\begin{aligned} |z_j^t\rangle &= \sigma_{QJS-Net}\left(\sum_j^{n \times m} f\left(\frac{\pi}{2} y_j^t\right) \langle \varphi_{ji}^t | \xi_j^t \rangle\right) \\ &= \sigma_{QJS-Net}\left(\sum_j^{n \times m} f\left(\frac{\pi}{2} \times \sigma_{QJS-Net}\left(\sum_l^{n \times m} f\left(\frac{\pi}{2} y_l^t\right) \langle \varphi_{lj}^t | \xi_l^t \rangle\right)\right) \langle \varphi_{ji}^t | \xi_j^t \rangle\right) \end{aligned} \quad (25)$$

i.e.,

$$\begin{aligned} |z_j^t\rangle &= \sigma_{QJS-Net}\left(\sum_j^{n \times m} f\left(\frac{\pi}{2} \times \sigma_{QJS-Net}\left(\sum_l^{n \times m} f\left(\frac{\pi}{2} y_l^t\right) \cos(\omega_{lj}^t - v_l^t) \right.\right. \right. \\ &\quad \left.\left.\left. \cos(\omega_{ji}^t - v_j^t) + \tau \sin(\omega_{lj}^t - v_l^t) \sin(\omega_{ji}^t - v_j^t)\right)\right)\right) \end{aligned} \quad (26)$$

where τ is an imaginary unit.

The notable feature of the proposed QIS-Net architecture lies in fact that the processing in the intermediate and output layers are governed by the quantum multi-level sigmoidal activation with various thresholding measures.

4.2. Quantum-inspired multi-level sigmoidal (QMSig) activation function

The bi-level quantum activation function employed in the QBDSONN architecture [9,10] is replicated for each gray scale present in the image and thereby formed a novel quantum-inspired multi-level sigmoidal activation (QMSig) function embedded in the suggested QIS-Net quantum neural network model architecture. The suggested QMSig activation function incorporates various adaptive activation scheme. Hence, the quantum inspired multi-level sigmoidal (QMSig) activation function is effective for multi-polar gray scale image segmentation exploring multi-intensity gray scales and such QMSig function is employed in the QIS-Net architecture for efficient segmentation. The QMSig activation function is defined as:

$$\sigma_{QJS-Net}(x) = \frac{1}{\lambda_\omega + e^{-v(x-\eta)}} \quad (27)$$

where, $\sigma_{QJS-Net}$ is the quantum multi-level sigmoidal (QMSig) activation function with steepness factor v and activation value η represented by qbits and λ_ω exhibits the response of multi-level class. Given, the gray scale intensity index as λ_ω ($1 \leq \lambda_\omega \leq L$) where ω is the cluster index, λ_ω is defined as:

$$\lambda_\omega = \frac{S_N}{S_\omega - S_{\omega-1}} \quad (28)$$

where, ω^{th} and $\omega - 1^{th}$ class outputs designated by the containment of s_ω and $s_{\omega-1}$ in quantum environment and S_N is the contribution of 8-connected neighborhood gray-scale pixels as qbits.

The QMSig activation function given in Eq. (27) can be modified to a generalized QMSig function with the help of suitable tailoring of λ_ω and exhibits different subnormal response σ_{λ_ω} in quantum environment where $0 \leq \sigma_{\lambda_\omega} \leq \frac{\pi}{2}$. These subnormal responses co-jointly superimposed yields multi-level response in

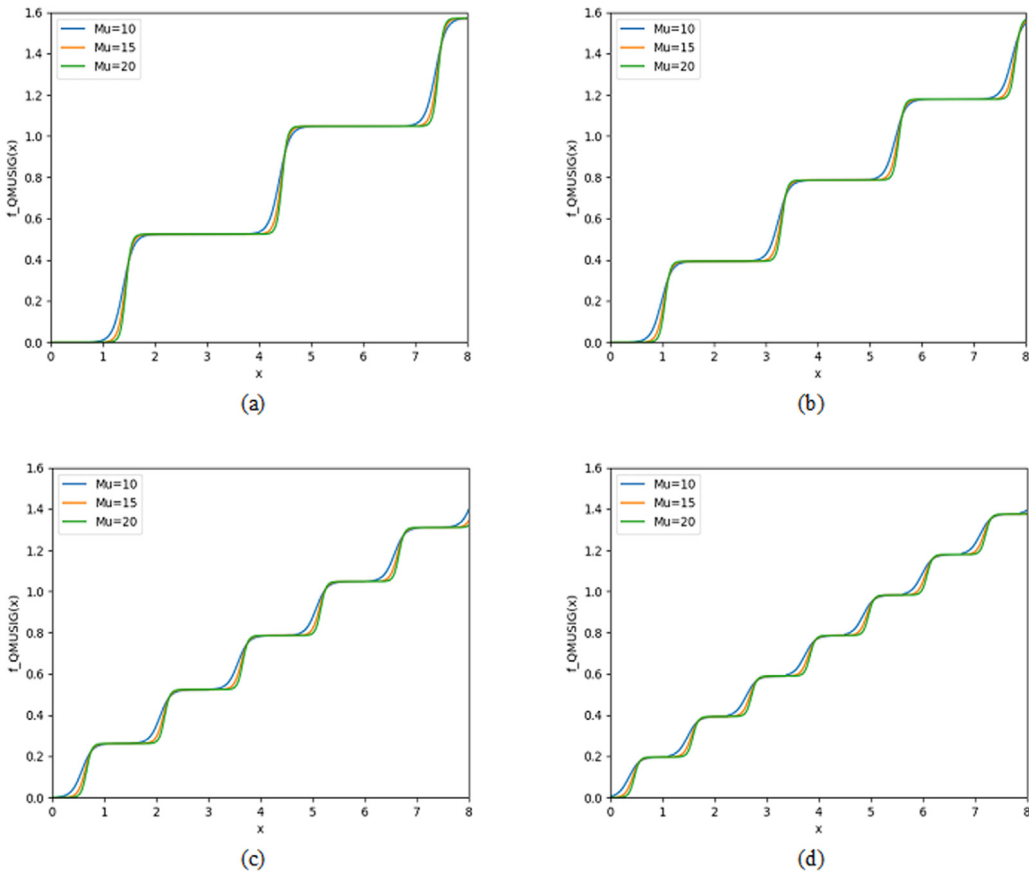


Fig. 2. Responses of Multi-class level QMSig activation function for $\mu = 10, 15, 20$ for distinct class boundaries (a) $L = 4$, (b) $L = 5$, (c) $L = 7$, (d) $L = 8$.

terms of quantum state using the generalized QMSig activation function defined as:

$$\sigma_{QIS-Net}(x; \lambda_\omega, s_\omega) = \frac{1}{\lambda_\omega + e^{-\nu(x-(\omega-1)s_{\omega-1}-\eta)}} \quad (29)$$

In order to maintain the continuity of the resultant QMSig function, several subnormal lobes are obtained varying with λ_ω in quantum state. Eq. (30) ensures that the number of distinct λ_ω parameters as same as number of classes ($L - 1$). The closed form of the resultant QMSig function is given as:

$$\sigma_R(x) = \sum_{\omega=1}^L \sigma_{QIS-Net}(x + (\omega - 1)s_{\omega-1}); \quad (30)$$

$$(\omega - 1)s_{\omega-1} \leq x \leq \omega s_\omega$$

Eq. (30) can be modified by substituting Eq. (29) as:

$$\sigma_R(x; \lambda_\omega, s_\omega) = \sum_{\omega=1}^L \frac{1}{\lambda_\omega + e^{-\nu(x-(\omega-1)s_{\omega-1}-\eta)}} \quad (31)$$

The QMSig activation functions with different hyper-parameters are provided in Fig. 2. Since the outputs generated at the output layer neurons of the QIS-Net architecture are in the quantum states, a quantum observation permits the quantum states to transform into classical bits to either 0 or 1 on interaction with the environment as given by Eq. (24). Final outcomes are obtained once the network attains stability or converge, otherwise, these quantum outputs undergoes further processing and are fed back to the intermediate layer through the counter path interconnections.

4.3. Updating inter-connection weight

Single quantum rotation gate offers the updating process of the interconnection strengths of the inter-layer inter-connections and the activation in form of qubits as follows:

$$|\varphi^{t+1}\rangle = \begin{pmatrix} \cos\Delta\alpha & -\sin\Delta\alpha \\ \sin\Delta\alpha & \cos\Delta\alpha \end{pmatrix} |\varphi^t\rangle \quad (32)$$

$$|\xi^{t+1}\rangle = \begin{pmatrix} \cos\Delta\gamma & -\sin\Delta\gamma \\ \sin\Delta\gamma & \cos\Delta\gamma \end{pmatrix} |\xi^t\rangle \quad (33)$$

where

$$\alpha^{t+1} = \alpha^t + \Delta\alpha^t \quad (34)$$

and

$$\gamma^{t+1} = \gamma^t + \Delta\gamma^t \quad (35)$$

The convergence or stability of the proposed self-organizing procedure with the QMSig activation function lies in advocating the angle of rotations $\Delta\alpha^t$ and $\Delta\gamma^t$ and are evaluated according to the Eqs. (18) and (19) respectively. This embedded novel feature of the self-supervised algorithm facilitates the sequence of epochs as given in Eqs. (34)–(35) to converge super-linearly [9]. To attain stability of the proposed self-supervised network, the network operation must converge super linearly as shown in Fig. 3. The network error in QIS-Net is evaluated as linear indices of fuzziness after quantum observation at output layer as follows [9]:

$$\zeta = \frac{1}{2} \sum (\vartheta^{t+1} - \vartheta^t)^2 \quad (36)$$

The quantum observation procedure converts the quantum interconnection weights $|\varphi^t\rangle$ in to ϑ^t at a particular epoch (t). It is

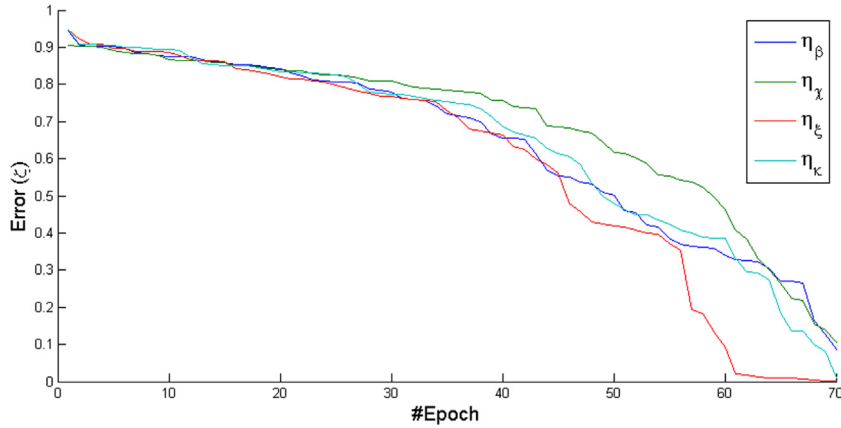


Fig. 3. Convergence Graph of the proposed QIS-Net for four different activation.

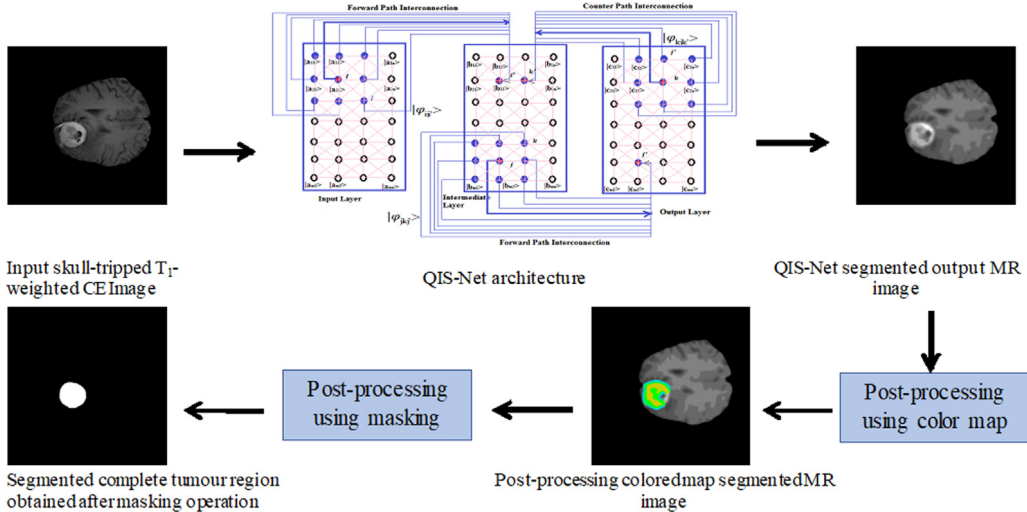


Fig. 4. Proposed quantum-inspired self-supervised integrated framework using QIS-Net architecture for fully automatic segmentation of Brain MR images.

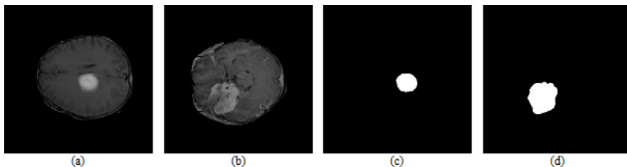


Fig. 5. Skull tripped Input Dynamic Susceptibility Contrast (DSC) brain MR images with size 512×512 (a) slice #10 (b) slice #2 (c) Manually annotated tumor for slice #10 and (d) for slice#2 [12].

evident from the aforementioned equation that α and γ describe the coherent error function ζ .

5. MR image segmentation using the proposed QIS-Net

The proposed QIS-Net receives the input MR image pixel information and it transforms the fuzzified information with various gray scales into quantum phase $q_i [0, \frac{\pi}{2}]$ as

$$q_i = \frac{\pi}{2} I_i \quad (37)$$

The fixed activation parameter η employed in the quantum inspired multi-level sigmoidal (QMSig) activation function is suitable for uniformly distributed intensity images. However, due to wide variations of gray levels in image pixels, MR images exhibits

heterogeneous responses over the 8-connected neighborhoods. Hence, adaptive thresholding schemes [40] have received great attention where adaptivity relies on the intensity information over the neighborhood pixels. The MR image information is processed through the different layer of neurons in quantum phase. These q bits information in the form of fuzzified gray scales undergoes the application of the QMSig function with varying adaptive parameters of activation η . In this paper, there are four different adaptive thresholding based activation schemes are extended in quantum environment [40].

- (1) β -distributed intensity of 8-connected neighborhood image pixel (η_β) based activation
- (2) Activation based on Skewness (η_χ)
- (3) 8-connected quantum fuzzy pixel information heterogeneity assisted activation (η_ξ)
- (4) 8-connected quantum fuzzy cardinality estimation guided activation (η_κ)

The multi-class gray-level transition (L_ω) for fixed class L can be defined in a set F_{λ_ω} as

$$F_{\lambda_\omega L} = \{\{f_{\lambda_\omega L}\}, L = 4, 5, 6, 7, 8\} \quad (38)$$

In this current work, for each multi-class level $L = \{4, 5, 6, 7, 8\}$ four sets $F_{\lambda_\omega L} = \{f_1, f_2, f_3, f_4\}$ of class boundary defined in the quantum state $[0, \frac{\pi}{2}]$. One set of such example is given below.

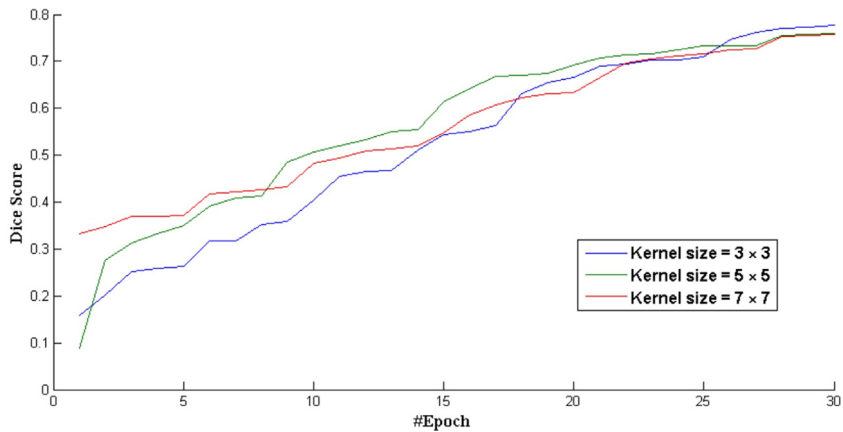


Fig. 6. Average Dice similarity reported using U-Net [23] for various kernel size during training for 30 epochs.

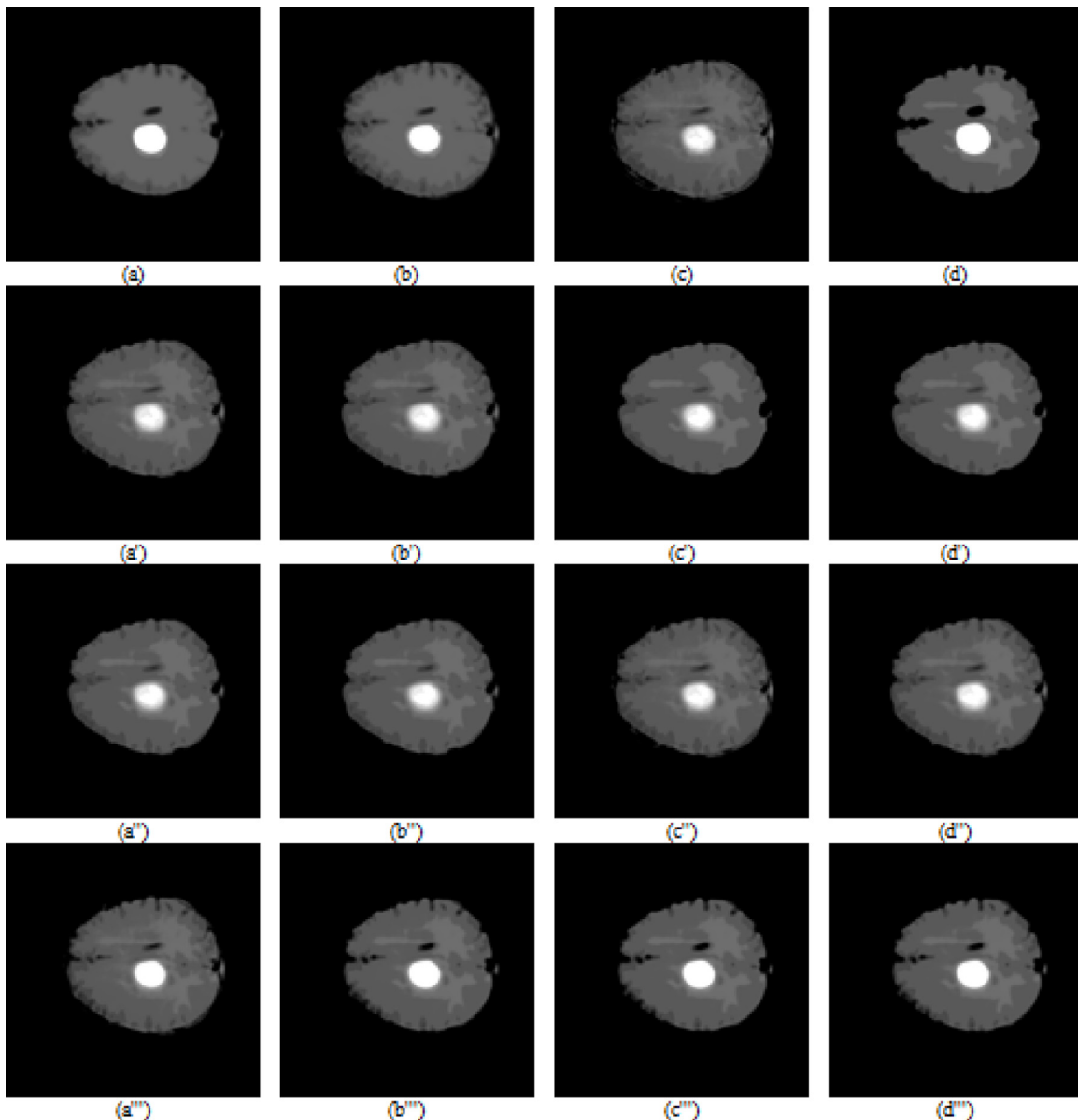


Fig. 7. Segmented output images using proposed QIS-Net architecture obtained from slice #10 using $L = 8$ transition levels with four different thresholding schemes $(a - a'')$ for η_β , $(b - b'')$ for η_χ , $(c - c'')$ for η_ξ and $(d - d'')$ for η_v with level set $(a - d)$ using f_1 , $(a' - d')$ using f_2 , $(a'' - d'')$ using f_3 , $(a''' - d''')$ using f_4 .

Table 1

Results obtained using proposed QIS-Net for the slice #10.

Level	Set	ACC				DSC				PPV				SS			
		η_β	η_χ	η_ξ	η_κ												
$L = 4$	f_1	0.99	0.99	0.99	0.98	0.45	0.48	0.46	0.34	0.31	0.33	0.30	0.21	0.85	0.88	0.94	0.95
	f_2	0.99	0.95	0.99	0.97	0.45	0.14	0.75	0.21	0.29	0.08	0.70	0.11	0.94	0.97	0.81	0.97
	f_3	0.97	0.97	0.98	0.96	0.21	0.23	0.35	0.45	0.11	0.13	0.22	0.30	0.97	0.97	0.96	0.92
	f_4	0.95	0.93	0.97	0.89	0.41	0.35	0.39	0.37	0.25	0.21	0.24	0.22	0.99	0.99	0.91	0.99
$L = 5$	f_1	0.99	0.99	0.99	0.99	0.80	0.82	0.80	0.79	0.69	0.76	0.70	0.68	0.94	0.89	0.93	0.94
	f_2	0.99	0.99	0.99	0.99	0.84	0.82	0.82	0.83	0.80	0.76	0.84	0.76	0.89	0.89	0.82	0.94
	f_3	0.99	0.99	0.99	0.99	0.82	0.82	0.80	0.79	0.78	0.76	0.71	0.70	0.86	0.89	0.91	0.94
	f_4	0.69	0.69	0.69	0.69	0.25	0.24	0.24	0.24	0.12	0.12	0.12	0.94	0.94	0.92	0.91	0.91
$L = 6$	f_1	0.99	0.99	0.99	0.99	0.80	0.79	0.80	0.79	0.73	0.68	0.73	0.69	0.89	0.94	0.89	0.92
	f_2	0.99	0.99	0.99	0.99	0.81	0.80	0.81	0.79	0.72	0.72	0.74	0.69	0.91	0.89	0.89	0.94
	f_3	0.99	0.99	0.99	0.99	0.71	0.73	0.72	0.71	0.55	0.58	0.57	0.56	0.97	0.96	0.96	0.96
	f_4	0.71	0.71	0.72	0.71	0.02	0.02	0.02	0.02	0.01	0.01	0.01	0.99	0.99	0.92	0.97	0.97
$L = 7$	f_1	0.99	0.99	0.99	0.99	0.79	0.79	0.80	0.80	0.68	0.68	0.73	0.72	0.94	0.94	0.89	0.89
	f_2	0.99	0.99	0.99	0.99	0.81	0.81	0.80	0.80	0.72	0.72	0.72	0.70	0.92	0.92	0.92	0.93
	f_3	0.99	0.99	0.99	0.99	0.79	0.79	0.79	0.80	0.68	0.68	0.69	0.74	0.94	0.88	0.92	0.87
	f_4	0.99	0.99	0.99	0.99	0.79	0.79	0.79	0.80	0.68	0.69	0.68	0.72	0.88	0.92	0.94	0.89
$L = 8$	f_1	0.99	0.99	0.99	0.99	0.77	0.55	0.80	0.75	0.65	0.37	0.69	0.61	0.97	0.99	0.94	0.97
	f_2	0.99	0.99	0.99	0.99	0.46	0.49	0.74	0.72	0.30	0.32	0.60	0.57	0.99	0.92	0.98	0.99
	f_3	0.99	0.99	0.99	0.99	0.79	0.79	0.80	0.79	0.68	0.69	0.70	0.68	0.94	0.97	0.91	0.94
	f_4	0.99	0.99	0.99	0.99	0.79	0.79	0.81	0.81	0.69	0.69	0.70	0.70	0.94	0.92	0.94	0.94

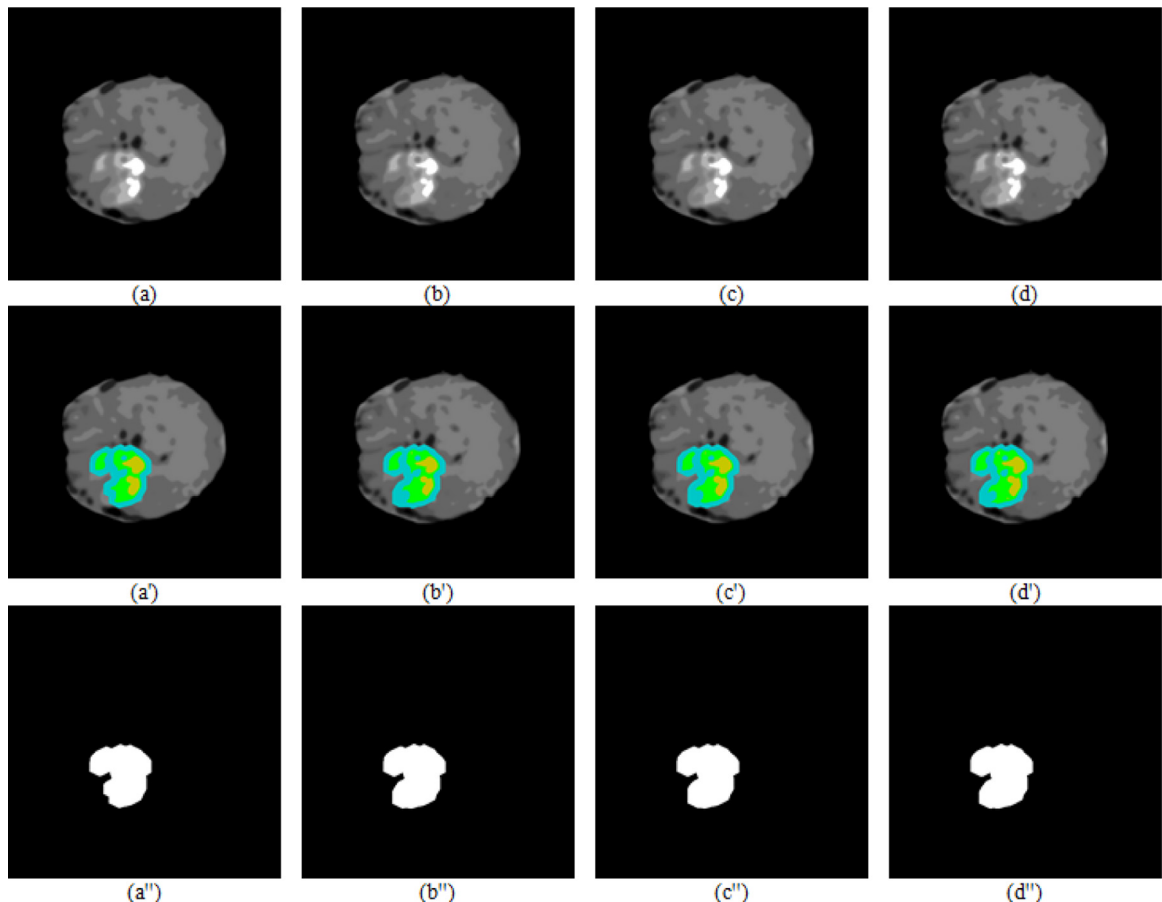


Fig. 8. (a – d) Segmented output images, (a' – d') Post processed with color map (Core Tumor-Yellow, Complete Tumor-Green and Edema region-Sky blue) and (a'' – d'') Post processed output images with binary masking using QIS-Net on slice #2 using $L = 8, f_1$ transition levels with four different thresholding schemes η_β ($a - a''$), η_χ ($b - b''$), η_ξ ($c - c''$) and η_ν ($d - d''$) from slice #2 using $L = 8, f_1$.

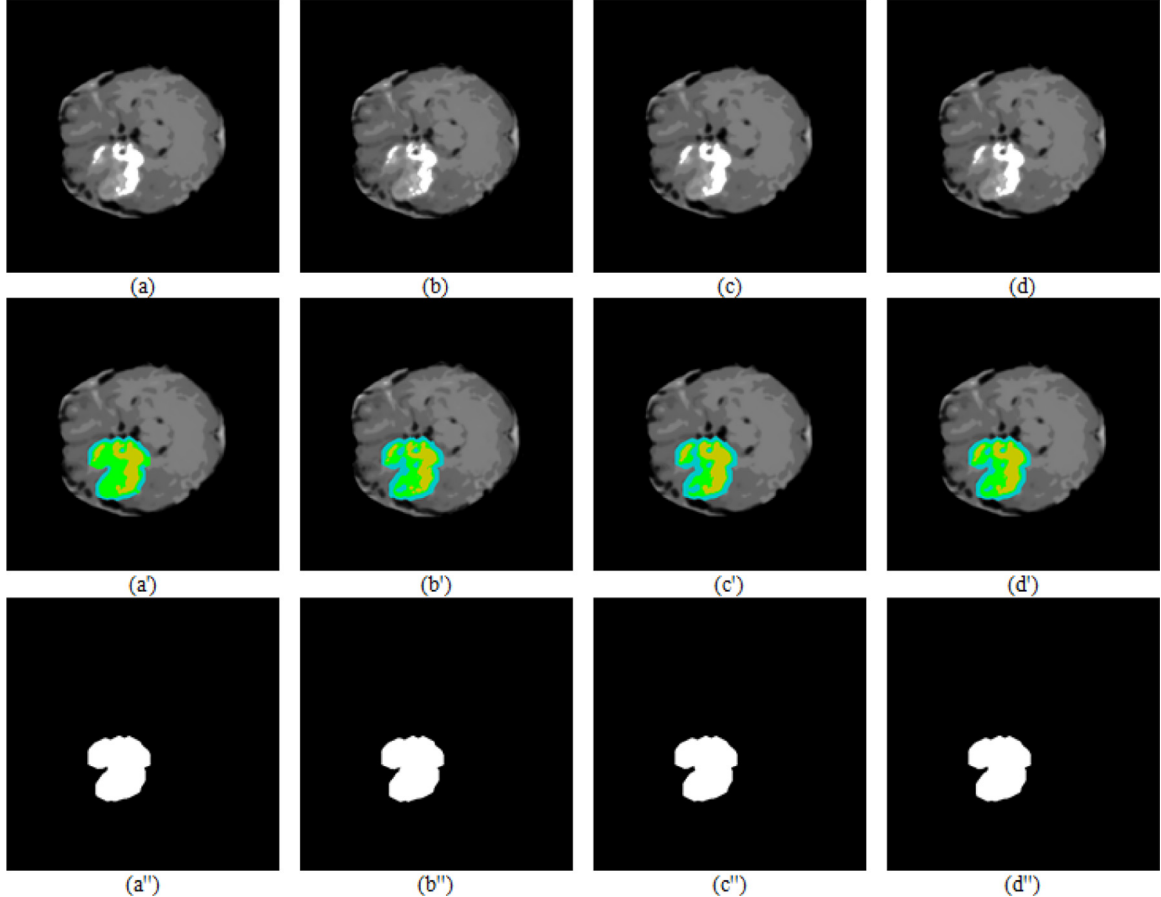


Fig. 9. (a – d) Segmented output images, (a' – d') Post processed with color map (Core Tumor-Yellow, Complete Tumor-Green and Edema region-Sky blue) and (a'' – d'') Post processed output images with binary masking using QIS-Net on slice #2 using $L = 8, f_1$ transition levels with four different thresholding schemes η_β (a – a''), η_χ (b – b''), η_ξ (c – c'') and η_ν (d – d'') from slice #2 using $L = 8, f_2$.

$$\begin{aligned} F_{\lambda_{\omega(8)}} = \frac{\pi}{2} \times & \{ \{0, 0.15, 0.29, 0.43, 0.57, 0.71, 0.85, 1], \\ & \{0, 0.16, 0.30, 0.44, 0.58, 0.72, 0.86, 1], \\ & \{0, 0.15, 0.30, 0.45, 0.60, 0.75, 0.90, 1], \\ & \{0, 0.16, 0.31, 0.46, 0.61, 0.76, 0.91, 1] \} \end{aligned} \quad (39)$$

The multi-level class response (λ_ω) is observed to rely on the context sensitive information of 8-connected neighborhood (S_N) expressed as *qbits* and the cluster transition levels (L_ω). The standard empirical goodness evaluation (PPV, SS, ACC, DSC) scheme has been used to measure the accuracy of the experimental outcomes as stated in 6.2 with four different thresholding ($\eta_\beta, \eta_\chi, \eta_\xi, \eta_\nu$) for different level sets. An integrated self-supervised framework using QIS-Net architecture for fully automatic segmentation of Brain MR images is illustrated in Fig. 4.

6. Results and discussion

6.1. Data set

Dynamic Susceptibility Contrast (DSC) MR image segmentation for brain tumor detection is performed using QIS-Net characterized by the suggested quantum-inspired network model with QMSig activation function. The Dynamic Susceptibility Contrast (DSC) brain MR images are collected from Nature data sets [12]. The proposed quantum-inspired self-supervised procedure using

QIS-Net with adaptive thresholding schemes, the unsupervised fuzzy-C-means clustering (FCM) [17] and the self-supervised network models QIBDS Net [11] and Opti-QIBDS Net [34] are tested on 800 Dynamic Susceptibility Contrast (DSC) brain MR images. The U-Net [23], FCNN-2 [20] and FCNN-4 [20] are trained using stochastic gradient descent algorithm with learning rate as 0.01 with randomly chosen images as training, validation and test images of size 2000, 264 and 800 Dynamic Susceptibility Contrast (DSC) brain MR images respectively.

6.2. Evaluation criteria

Pereira et al. [19] suggested an evaluation scheme based on four viz. matrices Positive Predictive Value (PPV), Sensitivity (SS), Accuracy (ACC) and Dice Similarity Score (DSC). The similarity between the segmented MR images and the ground truth images are evaluated using DSC. Given, T_{RP} = True Positive, F_{LP} = False Positive, T_{RN} = True Negative and F_{LN} = False Negative, the evaluation matrices are defined as [19]:

$$PPV = \frac{T_{RP}}{T_{RP} + F_{LP}} \quad (40)$$

$$SS = \frac{T_{RP}}{T_{RP} + F_{LN}} \quad (41)$$

$$ACC = \frac{T_{RP} + T_{RN}}{T_{RP} + F_{LP} + T_{RN} + F_{LN}} \quad (42)$$

$$DSC = \frac{2T_{RP}}{2T_{RP} + F_{LP} + F_{LN}} \quad (43)$$

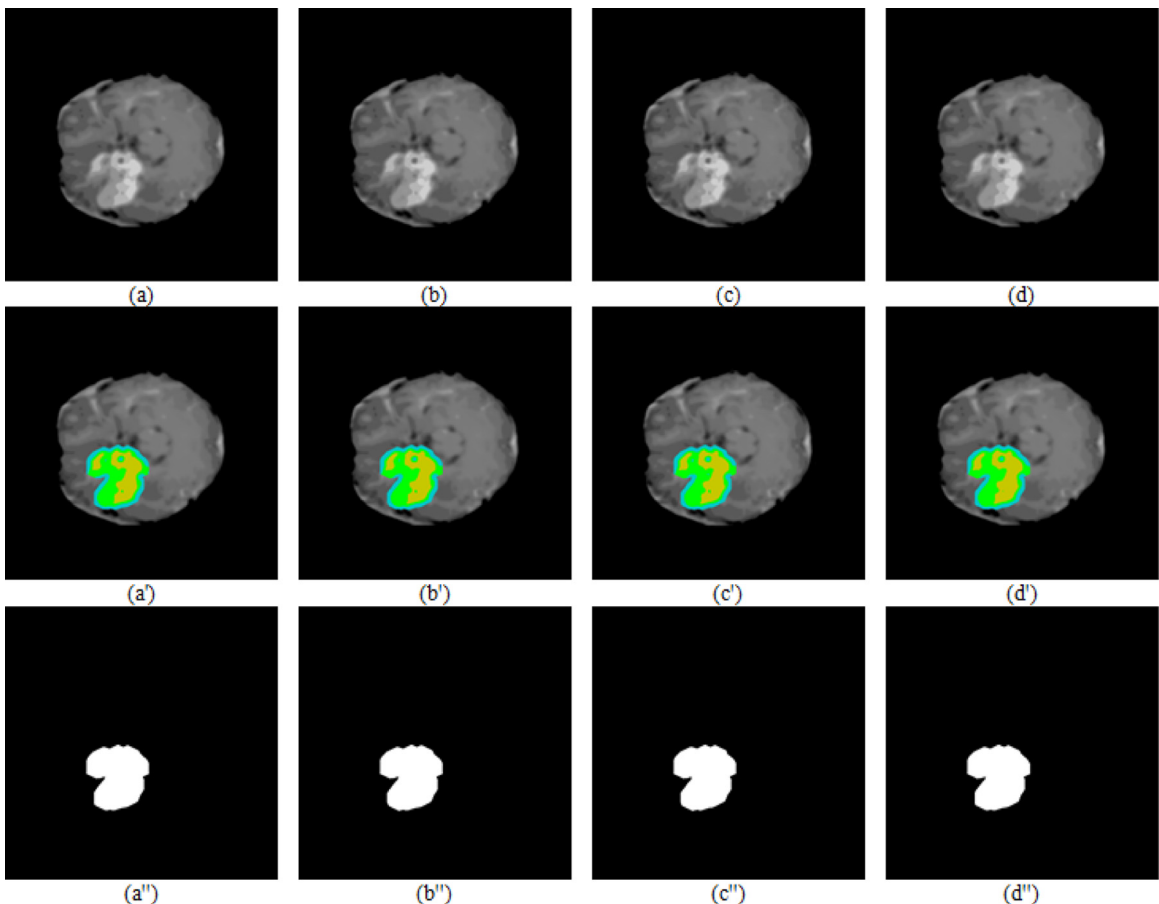


Fig. 10. (*a* – *d*) Segmented output images, (*a'* – *d'*) Post processed with color map (Core Tumor-Yellow, Complete Tumor-Green and Edema region-Sky blue) and (*a''* – *d''*) Post processed output images with binary masking using QIS-Net on slice #2 using $L = 8, f_1$ transition levels with four different thresholding schemes η_β (*a* – *a''*), η_χ (*b* – *b''*), η_ξ (*c* – *c''*) and η_ν (*d* – *d''*) from slice #2 using $L = 8, f_3$.

In addition, we have also conducted Kolmogorov-Smirnov test (KS-test) to measure statistical significance of the outcome obtained from the experiments. One-sided KS-test is chosen since the distribution of the experimental output observations is unknown in prior and non-parametric in nature. In contrast to comparative analysis of two distinct samples, Empirical Cumulative Distribution Functions (ECDF) throws light in to the statistical dissimilarity between two sets of outcome. Null hypothesis H_0 and alternative hypothesis H_t are the significant players in KS test. If two data samples X and Y are obtained from similar distribution or they are statistically equal ($X = Y$) then it is known as Null hypothesis. On the contrary, if the data distributions differ or they are statistically dissimilar ($<$ or $>$) then it is defined as alternative hypothesis. Interested researchers may mitigate [9,41,42] to explore more details about KS-test.

6.3. Experimental setup

Rigorous experiments have been carried out on 3064 Dynamic Susceptibility Contrast (DSC) brain MR images (which includes 2000 slices for training, 264 for validation and 800 for testing) of size 512×512 . We have employed RTX 2070 Nvidia Graphics processor for training the U-Net and FCNN networks. On the contrary, implemented QIS-Net, QIBDS Net, Opti-QIBDS Net in Matlab 2019 with 8 GB RAM, 3.2 GH Processor without any additional Graphics Processing Unit. The QIS-Net, QIBDS Net and Opti-QIBDS Net all are characterized with four different thresholding schemes

Table 2

Comparative analysis of proposed QIS-Net with QIBDS Net, Opti-QIBDS Net, Fuzzy C-means clustering (FCM), FCNN-2, FCNN-4 and U-Net for threshold(η_ξ). [The optimal results are shown in bold].

Network	Set	ACC	DSC	PPV	SS	Avg.# of Epochs
QIS-Net	f_1	0.986	0.713	0.592	0.849	11.58
	f_2	0.985	0.718	0.563	0.930	11.58
	f_3	0.989	0.781	0.641	0.937	11.62
	f_4	0.990	0.780	0.637	0.951	12.02
QIBDS Net [11]	f_1	0.984	0.763	0.665	0.954	12.78
	f_2	0.985	0.765	0.720	0.960	14.55
	f_3	0.980	0.765	0.656	0.927	11.75
	f_4	0.989	0.763	0.657	0.961	12.06
Opti-QIBDS Net [34]	f_1	0.987	0.752	0.674	0.819	12.18
	f_2	0.986	0.758	0.683	0.955	12.15
	f_3	0.987	0.767	0.656	0.897	12.58
	f_4	0.990	0.770	0.683	0.876	13.73
FCNN-4 [20]		0.987	0.720	0.601	0.901	41.05
FCNN-2 [20]		0.987	0.722	0.612	0.904	37.83
U-Net [23]		0.991	0.792	0.685	0.945	18.95
FCM [17]		0.982	0.697	0.512	0.924	–

mentioned in Section 5. The experiment is also conducted with the same data set T_1 -weighted MR images using supervised Convolutional U-Net [23] with varying size of kernels $3 \times 3, 5 \times 5$ and

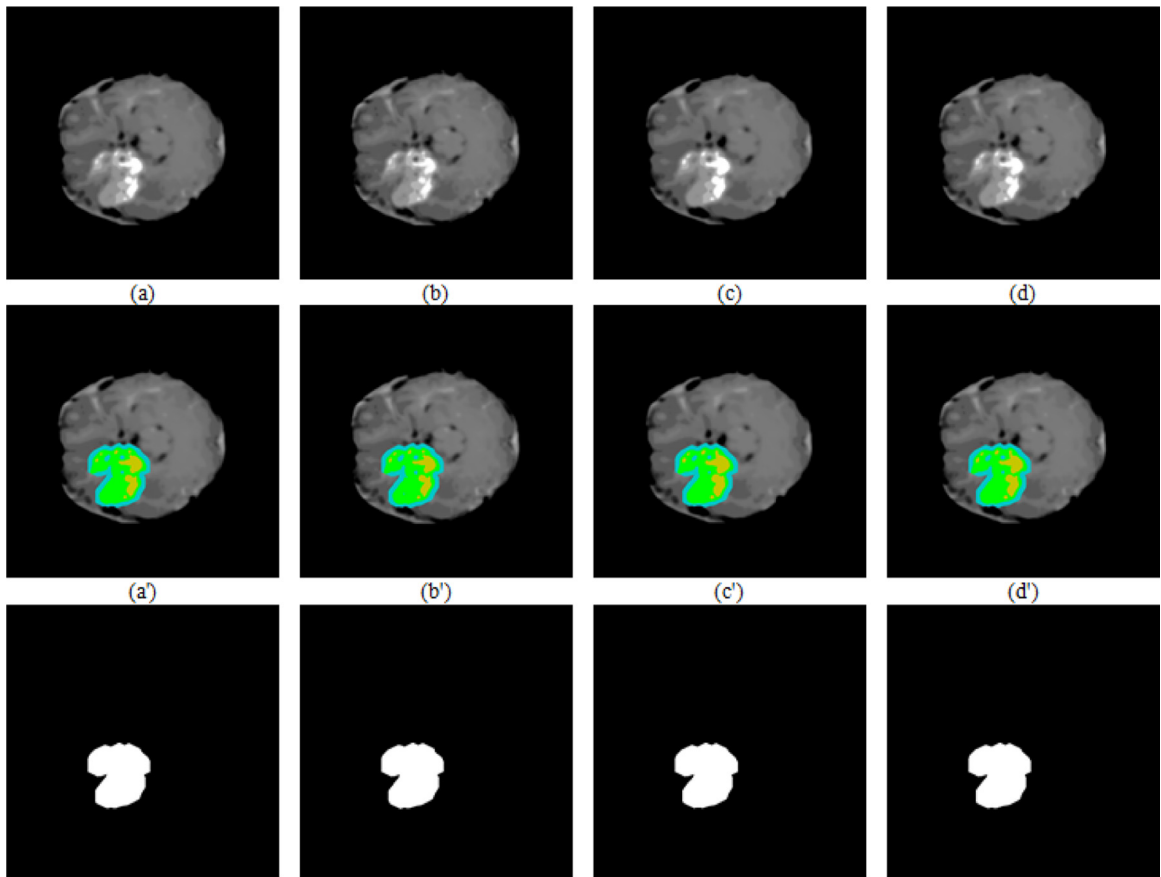


Fig. 11. (a – d) Segmented output images, (a' – d') Post processed with color map (Core Tumor-Yellow, Complete Tumor-Green and Edema region-Sky blue) and (d'' – d'') Post processed output images with binary masking using QIS-Net on slice #2 using $L = 8, f_1$ transition levels with four different thresholding schemes η_β (a – a''), η_χ (b – b''), η_ξ (c – c'') and η_ν (d – d'') from slice#2 using $L = 8, f_4$.



Fig. 12. Complete tumor segmentation (a) Fuzzy C-means clustering [17] (b)FCNN-4 [20] (c) FCNN-2 [20] and (d) U-Net [23] from slice #2.

Table 3

One sided non-parametric Kolmogorov Smirnov (KS) [42] test between the proposed QIS-Net and QIBDS Net, Opti-QIBDS Net, Fuzzy C-means clustering, FCNN-2, FCNN-4 and U-Net for threshold (η_ξ) with significance level $\alpha = 0.05$.

Network	Set	ACC	DSC	PPV	SS
QIBDS Net [11]	f_1	=	>	>	>
	f_2	=	>	>	>
	f_3	<	<	>	<
	f_4	=	<	>	>
Opti-QIBDS Net [34]	f_1	=	>	>	<
	f_2	=	>	>	>
	f_3	<	<	>	<
	f_4	=	<	>	>
FCNN-4 [20]		<	<	<	<
FCNN-2 [20]		<	<	<	<
U-Net [23]		=	=	>	<
FCM [17]		<	<	<	<

7×7 with stride size 2×2 . It has been found from the experiments that the kernel size 3×3 U-Net yields best performance as shown in Fig. 6. The proposed quantum-inspired self-supervised

procedure is also compared with the unsupervised fuzzy C-means clustering [17] for Brain image segmentation.

The proposed quantum inspired self-supervised procedure is tested on 800 test images by varying the gray level class response parameter λ_ω with distinct classes $L = 4, 5, 6, 7$ and 8 in the characterization of quantum multi-level sigmoidal (QMSig) activation function. The hyper parameter associated with QMSig activation function is steepness v which is varied from 0.23 to 0.24 with equal step size 0.001 during the experiments and optimal performance is observed for $v = 0.232$. It is a mentionable fact that all the segmented outcomes from Dynamic Susceptibility Contrast (DSC) brain MR input images of size 512×512 expose tiny regions as tumors erroneously. Hence, a post-processing procedure is being performed using a binary mask of equal size as input MR images. The removal of tiny clusters or regions with radius less than a threshold helps to reduce the number of false positive pixels. The Radius of the cluster (σ) is chosen intuitively and for $\sigma = 5$ pixels, after post processing the segmented output is found to be optimal while compared with the ground truth images.

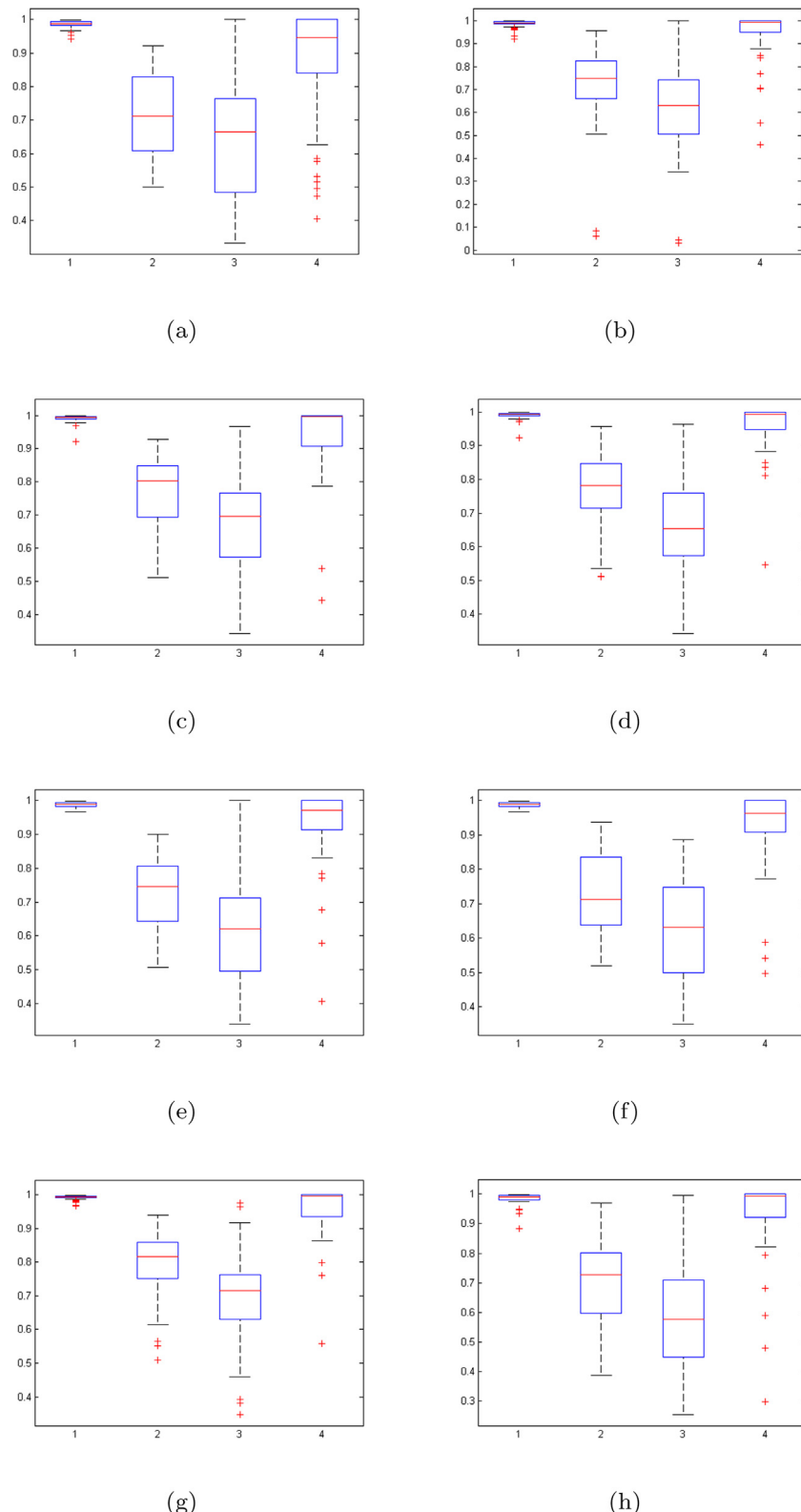


Fig. 13. Box plot of the results reported in Table 2 in the data set [12]. Boxplot of QIS-Net for different level sets of class boundary (a) f_1 , (b) f_2 , (c) f_3 and (d) f_4 respectively. Box plot for (e) FCNN-2, (f) FCNN-4, (g) U-Net and (h) Fuzzy-C-means (FCM) clustering respectively. 1 → Accuracy (ACC), 2 → Dice Score (DSC), 3 → PPV, 4 → Sensitivity (SS).

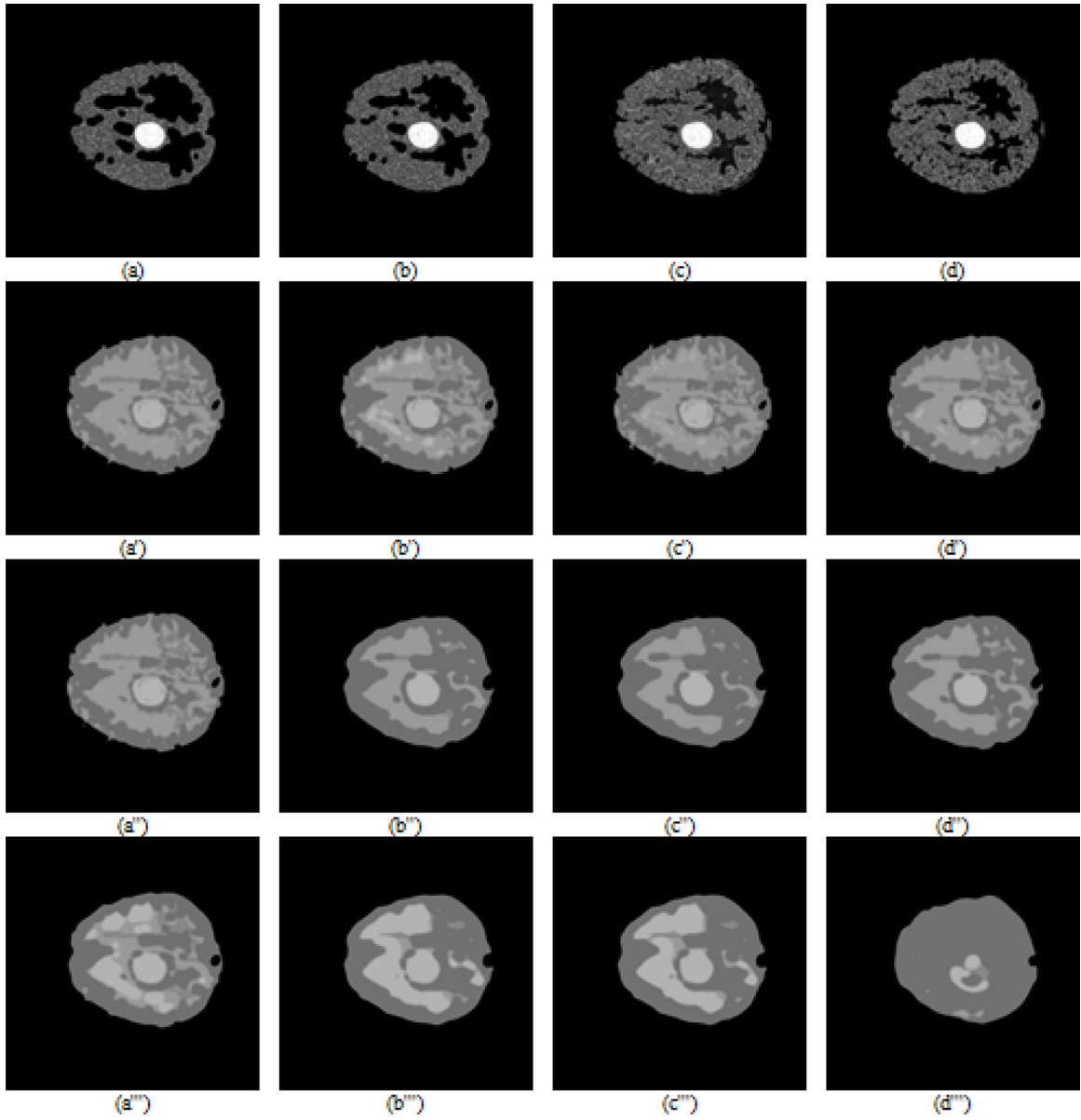


Fig. B.14. Segmented output images using proposed QIS-Net obtained from slice #10 using $L = 4$ transition levels with four different thresholding schemes ($a - a''$) for $\eta_{\theta\beta}$, ($b - b'''$) for η_χ , ($c - c'''$) for η_ξ and ($d - d'''$) for η_v with level set ($a - d$) using f_1 , ($a' - d'$) using f_2 , ($a'' - d''$) using f_3 , ($a''' - d'''$) using f_4 .

6.4. Experimental results

The experimental results on 800 test images are reported using the suggested quantum-inspired self-supervised QIS-Net architecture, QIBDS Net [11] and Opti-QIBDS Net [34] supervised convolutional U-Net [23], fully convolutional neural network architecture (FCNNs) [20] and unsupervised fuzzy C-means clustering [17]. The skull-tripped input slices with ground truth manually segmented tumors are given in Fig. 5 as examples. The segmented output images obtained using the proposed QIS-Net architecture from slice #10 using transition level ($L = 8$) with four different thresholding activation schemes have been demonstrated in Fig. 7. It is evident from the experimental data provided in Table 1 that the proposed QIS-Net performed optimally for 8-connected quantum fuzzy pixel information heterogeneity assisted activation (η_ξ) with $L = 8$ in comparison

with other thresholding schemes under four evaluation parameters PPV , SS , ACC , DSC . The segmented tumors obtained using the proposed self-supervised procedure under $L = 8$ class transition levels with four different thresholding schemes η_β , η_χ , η_ξ and η_v are demonstrated in Figs. 8–11 for four distinct gray scale sets f_1, f_2, f_3, f_4 respectively. The segmented tumor region using fuzzy C-means clustering, FCNNs and U-Net is also presented in Fig. 12.

Table 2 refers to the average accuracy (ACC), dice similarity score (DSC), positive prediction value (PPV), sensitivity (SS) and average number of epochs as reported by the proposed QIS-Net, QIBDS Net and Opti-QIBDS Net with class level $L = 8$ and activation (η_ξ) for all the four level sets f_1, f_2, f_3, f_4 . In addition, ACC , DSC , PPV and SS are also reported for supervised FCNN-4, FCNN-2, U-Net and unsupervised fuzzy C-means clustering as given in Table 2. The comparative analysis shows that the QIS-Net architecture with set f_4 and f_3 outperforms FCNN-4, FCNN-2

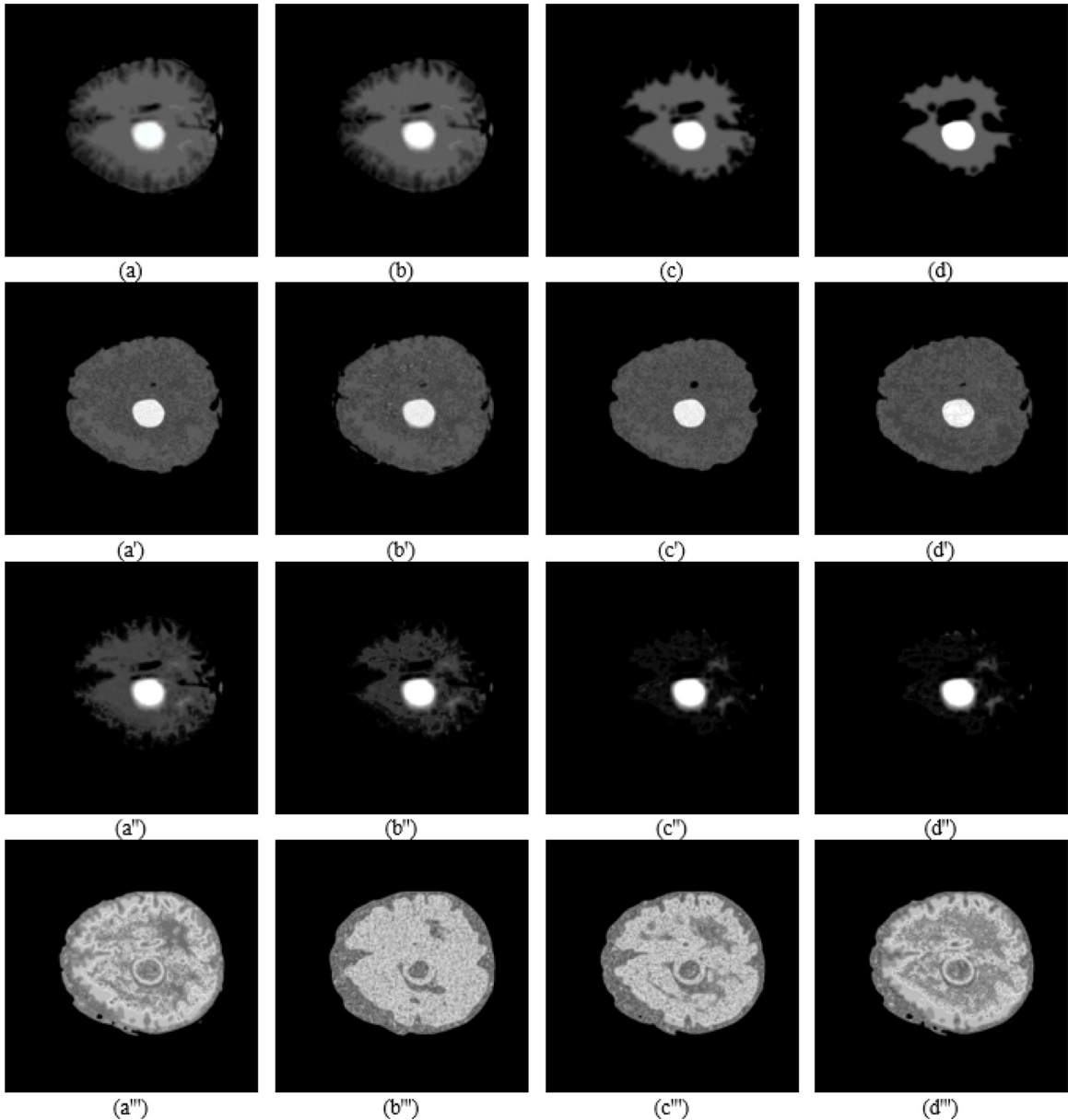


Fig. B.15. Segmented output images using proposed QJS-Net architecture obtained from slice #10 using $L = 5$ transition levels with four different thresholding schemes $(a - a'')$ for $\eta_{\theta\bar{\theta}}$, $(b - b'')$ for η_{χ} , $(c - c'')$ for $\eta_{\xi\bar{\xi}}$ and $(d - d'')$ for η_v , with level set $(a - d)$ using f_1 , $(a' - d')$ using f_2 , $(a'' - d'')$ using f_3 , $(a''' - d''')$ using f_4 .

and clustering approach in all aspects (*ACC*, *DSC*, *PPV* and *SS*). However, results reported using the supervised U-Net is superior to the proposed quantum-inspired self-supervised QIS-Net framework. The average number of epochs required to train U-Net and FCNNs allowing maximum 50 epochs are reported in the article. In addition, the average number of iterations required to obtain segmented image using QIS-Net, QIBDS Net and Opti-QIBDS Net are also reported in Table 2. The box plotting of dice similarity score of QIS-Net, U-net, FCNNs and FCM are demonstrated in Fig. 13. Moreover, one sided two sample Kolmogorov-Smirnov (KS) test [42] is also conducted with significance level $\alpha = 0.05$ to evaluate the statistical significance of the proposed self-supervised procedure with QIS-Net architecture and QIBDS Net, Opti-QIBDS Net, FCNNs, U-Net and fuzzy C-means clustering as presented in Table 3. The data presented in Table 2 is in sheer contrast to the numerical data obtained from experimental outcome. Keeping away these stray cases, it can be summarized, that the performance of the QIS-Net architecture on T_1 weighted

post enhanced MR images is statistically significant and superior than the QIBDS Net, Opti-QIBDS Net, FCNNs and fuzzy C-means clustering under comparison.

7. Conclusion

In this article, a Quantum-Inspired Self-Supervised Network (QIS-Net) architecture characterized by QMSig activation function has been proposed to promote fully automatic segmentation of Dynamic Susceptibility Contrast (DSC) brain MR images in real-time. The incorporation of quantum computing aims at providing better convergence of the QIS-Net resulting in fast and accurate MR image segmentation. The proposed quantum-inspired self-supervised procedure is the first novel attempt involving any self-organized neural network architecture for Brain MR image segmentation without external supervision and minimum human intervention. The efficacy of the QIS-Net architecture have

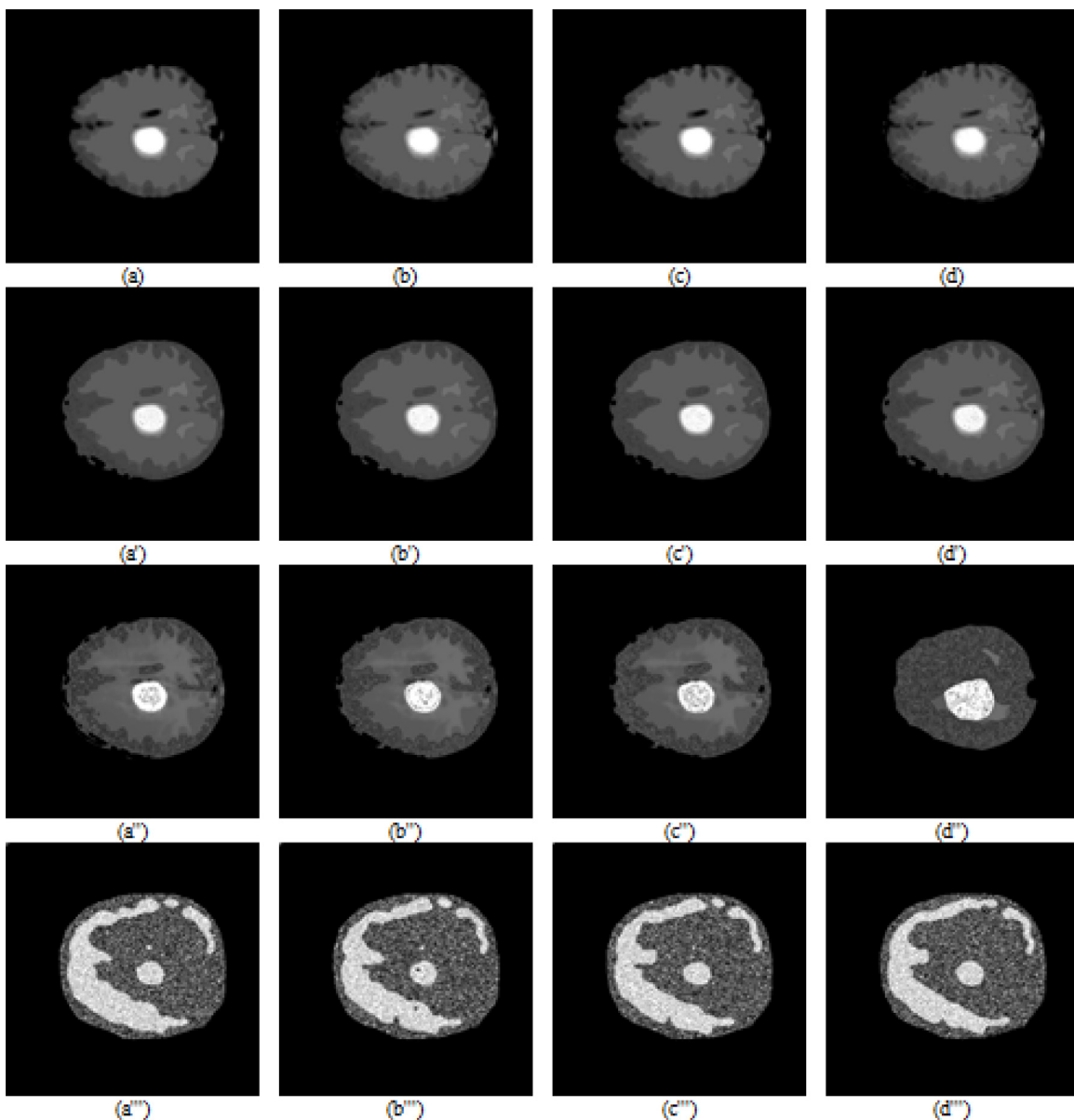


Fig. B.16. Segmented output images using proposed QIS-Net architecture obtained from slice #10 using $L = 6$ transition levels with four different thresholding schemes ($a - a''$) for η_{θ_β} , ($b - b''$) for η_χ , ($c - c''$) for η_ξ and ($d - d''$) for η_v with level set ($a - d$) using f_1 , ($a' - d'$) using f_2 , ($a'' - d''$) using f_3 , ($a''' - d'''$) using f_4 .

been demonstrated on the segmentation of Dynamic Susceptibility Contrast (DSC) brain MR images and compared with unsupervised fuzzy-clustering based approach and supervised convolutional neural network (CNN) and fully convolutional neural networks (FCNNs). In spite of adapting a self-supervised network architecture, QIS-Net reports similar pattern of accuracy as U-Net and outperforms QIBDS Net, Opti-QIBDS Net, FCNNs and fuzzy-C-means clustering. A little investigation using the statistical significance test (KS test) reveals that statistically U-Net and the proposed QIS-Net provides similar accuracy, dice similarity. In addition, QIS-Net requires very less computational overhead to implement in terms of processing time and resources compared with U-net and FCNNs which is evident from the required average number of epochs as reported in Table 2. It can be concluded from the experimental outcomes that the proposed self-supervised QIS-Net offers a promising alternative to the deeply supervised neural network architectures (U-Net and FCNNs) in medical image segmentation. Since, the proposed QIS-Net architecture provides multi-level segmented tumor outcomes, the

current quantum inspired network system architecture can be efficiently applied on any data set with multi-level gray scale manually segmented ground truth MR images. However, it remains to investigate the 3D version of the QIS-Net architecture applicable for volumetric MR image segmentation.

CRediT authorship contribution statement

Debanjan Konar: Conceptualization, Methodology, Software, Investigation, Validation, Writing - original draft. **Siddhartha Bhattacharyya:** Data curation, Writing - review & editing, Supervision. **Tapan Kr. Gandhi:** Supervision. **Bijaya Ketan Panigrahi:** Supervision.

Declaration of competing interest

The authors declare that they have no known competing financial interests or personal relationships that could have appeared to influence the work reported in this paper.

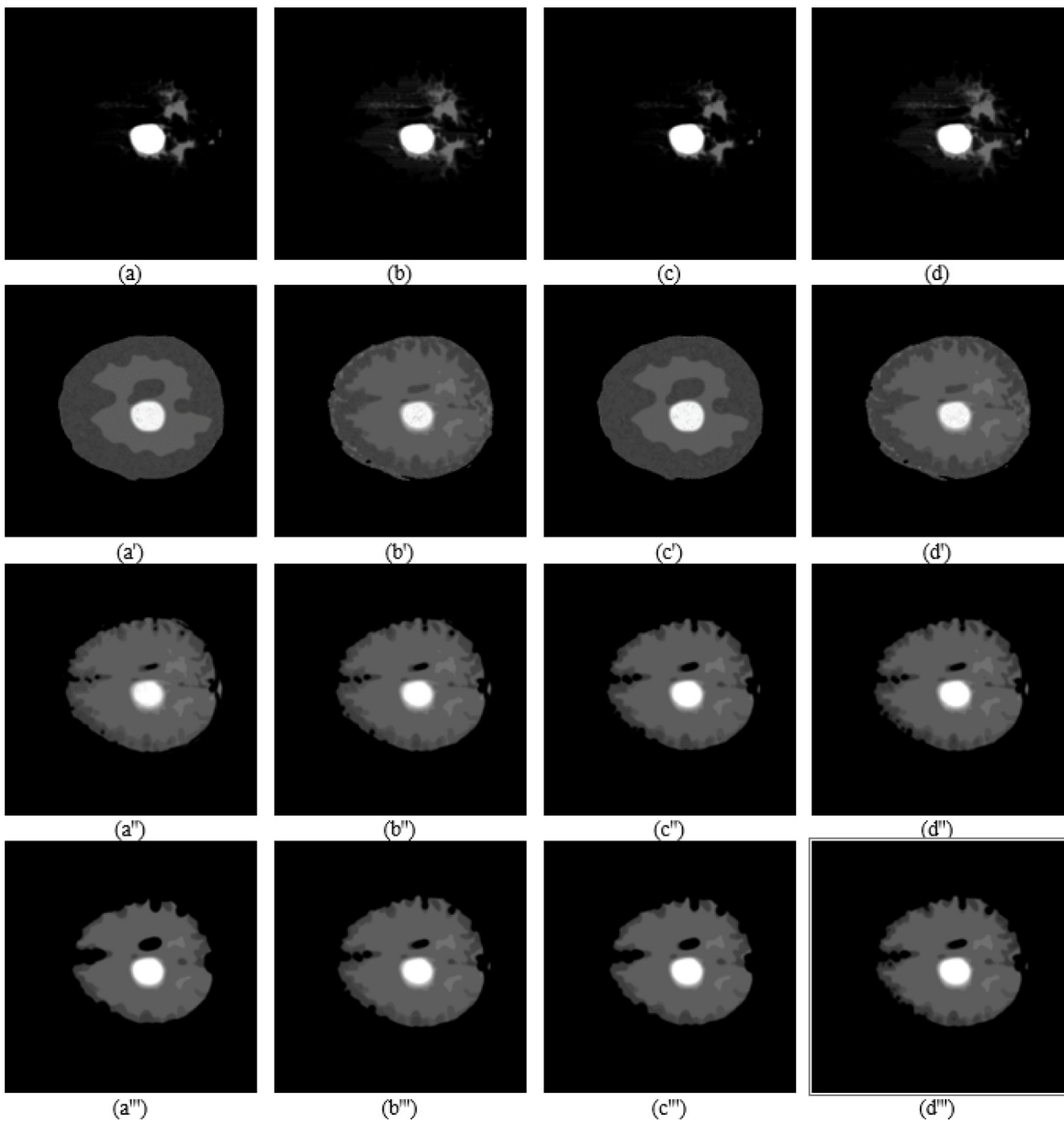


Fig. B.17. Segmented output images using proposed QIS-Net obtained from slice #10 using $L = 7$ transition levels with four different thresholding schemes ($a - a''$) for η_{θ_β} , ($b - b''$) for η_χ , ($c - c''$) for η_ξ and ($d - d''$) for η_v with level set ($a - d$) using f_1 , ($a' - d'$) using f_2 , ($a'' - d''$) using f_3 , ($a''' - d'''$) using f_4 .

Appendix A. Quantum-inspired Bi-directional self-supervision procedure

The proposed QIS-Net architecture is embedded with a quantum-inspired fully self-supervised and self-organized procedures and yields the segmented MR images. The quantum-inspired self-supervision algorithm is carried out in four subsequent phases: (i) QIS-Net initialization (ii) Input of quantum states (iii) forward propagation and (iv) counter propagation phase.

The quantum-inspired fully self-organized bi-directional algorithm embedded in the proposed QIS-Net is provided as follows.

Pseudo-code

1. Start

QIS-Net Initialization

2. Set the strength of intra-layer connections matrices $\Phi[l][i][j]$; ($l = 1, 2, 3, i = 1, \dots, M, j = 1, \dots, N$) to

unity for all trinity layers of the QIS-Net architecture to form cellular structure of each layer with unit weight.

Input of Quantum states

3. On receiving the raw image pixels from the input image of dimension $M \times N$ at the input layer of QIS-Net architecture, $\psi[l][i][j], l = 1, i = 1, \dots, M, j = 1, \dots, N$, the raw image pixel intensities are normalized to the fuzzified pixel information ([01]) as follows.

$$I[l][i][j] = X[l][i][j]/\max(X[l][i][j]), l = 1, i = 1, \dots, M, j = 1, \dots, N$$

4. The normalized fuzzified pixel intensities, $I[l][i][j], l = 1, i = 1, \dots, M, j = 1, \dots, N$ ([0, 1]) are transformed into input quantum states $[0, \frac{\pi}{2}]$ and treated as *qbuts* as follows.

$$\psi[l][i][j] = \frac{\pi}{2} \times I[l][i][j], l = 1, i = 1, \dots, M, j = 1, \dots, N$$

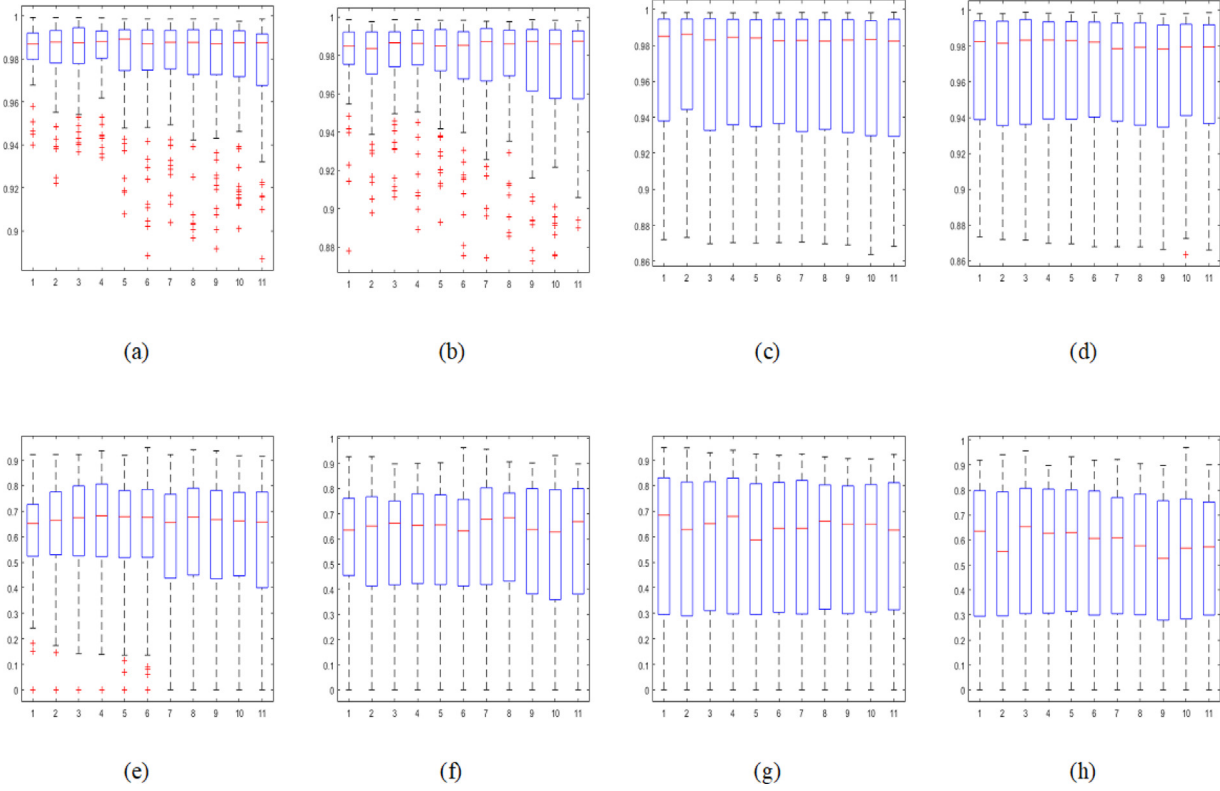


Fig. B.18. Box plot for QJS-Net for different level sets of class boundary (a & e) f_1 , (b & f) f_2 , (c & g) f_3 and (d & h) f_4 respectively for fixed class $L = 7$. (a–d) designates Accuracy (ACC) and (e–h) designates Dice Similarities (DSC). $1 \rightarrow v = 0.230$, $2 \rightarrow v = 0.231$, $3 \rightarrow v = 0.232$, $4 \rightarrow v = 0.233$, $5 \rightarrow v = 0.235$, $6 \rightarrow v = 0.235$, $7 \rightarrow v = 0.236$, $8 \rightarrow v = 0.237$, $9 \rightarrow v = 0.238$, $10 \rightarrow v = 0.239$, $11 \rightarrow v = 0.240$.

and the input layer of the QIS-Net architecture receives the input quantum states in the form of quantum fuzzified image pixels $\psi[l][i][j]$, $l = 1, i = 1, \dots, M, j = 1, \dots, N$.

Forward propagation phase

5. Set and update the angle of rotation for inter-linked weights between the layers of the QIS-Net and the activation at the inter-mediate and output layer as follows.

$$\alpha_{i,j} = 1 - (\psi[l][i][j] - \psi[l][i+p][j+q]), \quad l = 1, 2, 3, \\ i = 1, \dots, M, j = 1, \dots, N, \text{ and } p, q \in \{-1, 1\}$$

$$\gamma_i = 2\pi \times \sum_j \psi[l][i+p][j+q], \quad l = 1, 2, 3, i = 1, \dots, M, \\ j = 1, \dots, N, \text{ and } p, q \in \{-1, 1\}$$

$$|\varphi_{i,j,i'}\rangle = \begin{bmatrix} \cos(\frac{\pi}{2}\alpha_{i,j}) \\ \sin(\frac{\pi}{2}\alpha_{i,j}) \end{bmatrix} \\ |\xi_i\rangle = \begin{bmatrix} \cos\gamma_i \\ \sin\gamma_i \end{bmatrix}$$

where, $\psi[l][i][j]$ and $\psi[l][i+p][j+q]$ are the pixel intensity of the candidate pixel $[i, j]$ and one its 8-connected neighborhood pixel respectively for $l = 1, 2, 3, i = 1, \dots, M, j = 1, \dots, N$, and $p, q \in \{-1, 1\}$ in quantum formalism.

6. The inter-connection links are updated using the rotation gate as follows.

$$\varphi[\iota+1][l][l+1][i][j] = \begin{bmatrix} \cos(\frac{\pi}{2}\alpha) & -\sin(\frac{\pi}{2}\alpha) \\ \sin(\frac{\pi}{2}\alpha) & \cos(\frac{\pi}{2}\alpha) \end{bmatrix} \times \varphi[\iota][l][l+1][i][j]$$

where, the inter-linked weight between two successive layers l and $l+1$ at a particular iteration (ι) is $\varphi[\iota][l][l+1][i][j]$ for $l = 1, 2, 3, i = 1, \dots, M, j = 1, \dots, N$

7. The network output is computed as inner product of two matrices comprises processed input matrix and weight matrix guided by the Quantum-inspired Multi-level Sigmoidal activation function (QMSig) as

$$\psi[l+1][i][j] = \sum_{p=-1}^1 \sum_{q=-1}^1 [f_{QMSig}(\psi[l][i+p][j+q] * \varphi[\iota][l][l+1] \\ \times [i+p][j+q])], \quad \forall l = 1, 2, 3, i = 1, \dots, M, \\ j = 1, \dots, N$$

here, $*$ is the inner product operator which is defined as the sum of products of the entries of the matrices and imaginary or sin part is evaluated considering the quantum observation bit as 1 as follows.

$$x = (\psi[l][i+p][j+q] * \varphi[\iota][l][l+1][i+p][j+q]) \\ = \psi[l][i+p][j+q] \times \sin(\alpha_{i,j} - \gamma_i)$$

The Quantum-inspired Multi-level Sigmoidal activation function (QMSig) f_{QMSig} is defined as follows.

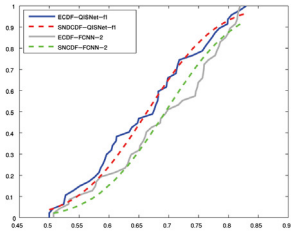
$$f_{QMSig} = \sum \frac{1}{\lambda_\omega + e^{-v(x-\eta)}}$$

and

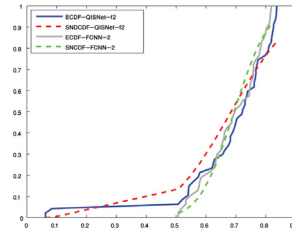
$$\lambda_\omega = \frac{S_N[l][i][j]}{\omega(t+1) - \omega(t)}, \quad \omega(t) \leq \psi[l][i][j] \leq \omega(t+1), \quad t = 1, \dots, 8$$

where

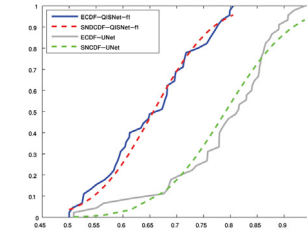
$$S_N[l][i][j] = \sum_{p=-1}^1 \sum_{q=-1}^1 \psi[l][i+p][j+q], \quad l = 1, 2, 3, i = 1, \dots, M,$$



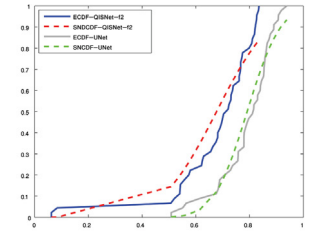
(a)



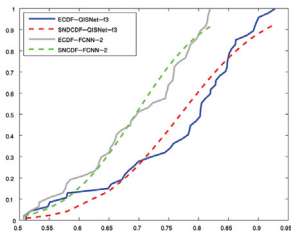
(b)



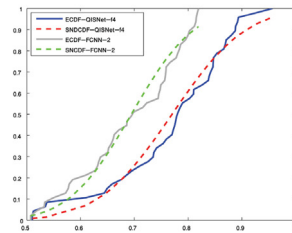
(a)



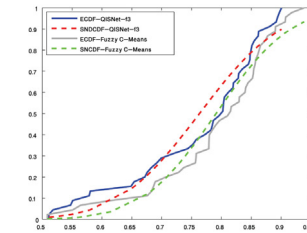
(b)



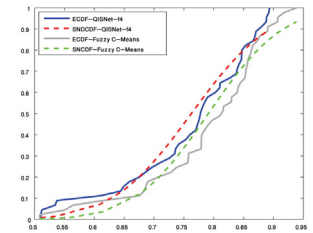
(c)



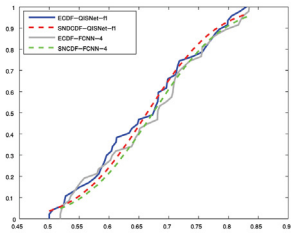
(d)



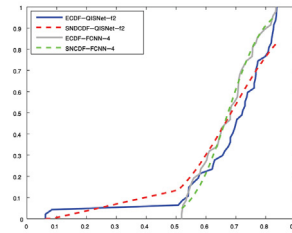
(a)



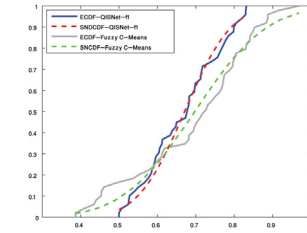
(b)



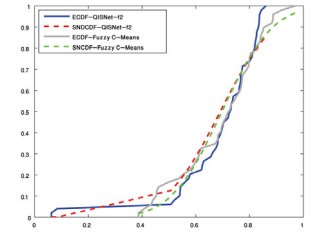
(e)



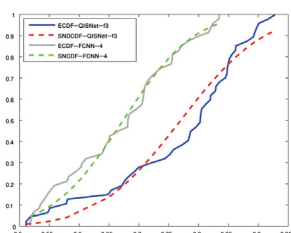
(f)



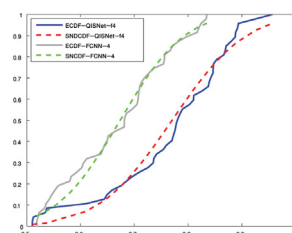
(e)



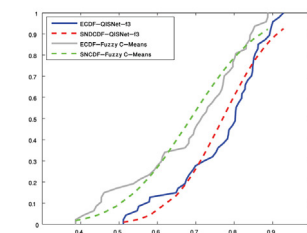
(f)



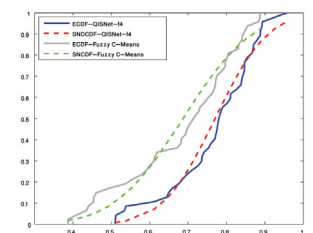
(g)



(h)



(e)



(f)

Fig. B.19. Empirical cdf (ECDF) and standard normal cdf (SNCDF) of Dice similarity (DSC) of proposed QIS-Net (for threshold(η_ξ)) and FCNN-2, FCNN-4 for all four sets $\{f_1, f_2, f_3, f_4\}$ are plotted in (a-d) and (e-h) respectively, where the data and cumulative probability are denoted by X and Y axes respectively.

Fig. B.20. Empirical cdf (ECDF) and standard normal cdf (SNCDF) of Dice similarity (DSC) of proposed QIS-Net (for threshold(η_ξ)) and U-Net and fuzzy-C-means (FCM) clustering for all four sets $\{f_1, f_2, f_3, f_4\}$ are plotted in (a-d) and (e-h) respectively, where the data and cumulative probability are denoted by X and Y axes respectively.

$$j = 1, \dots, N$$

8. Do

9. The hidden layer intermediate outcomes are repeated using the steps 5, 6, 7 in quantum formalism for successive operations as follows.

Counter propagation phase

10. Set and update the angle of rotation for inter-linked weights between the layers of the QIS-Net and the activation at the inter-mediate and output layer as follows.

$$\alpha_{i,j} = 1 - (\psi[l][i][j] - \psi[l][i+p][j+q]), l = 2, 3, i = 1, \dots, M,$$

$$j = 1, \dots, N, \text{ and } p, q \in \{-1, 1\}$$

$$\gamma_i = 2\pi \times \sum_j \psi[l][i+p][j+q], l = 2, 3, i = 1, \dots, M,$$

$$j = 1, \dots, N, \text{ and } p, q \in \{-1, 1\}$$

$$|\varphi_{i,j,i'}\rangle = \begin{bmatrix} \cos(\frac{\pi}{2}\alpha_{i,j}) \\ \sin(\frac{\pi}{2}\alpha_{i,j}) \end{bmatrix}$$

$$|\xi_i\rangle = \begin{bmatrix} \cos \gamma_i \\ \sin \gamma_i \end{bmatrix}$$

where, $\psi[l][i][j]$ and $\psi[l][i+p][j+q]$ are the pixel intensity of the candidate pixel $[i,j]$ and one its 8-connected neighborhood pixel respectively for $l = 2, 3, i = 1, \dots, M, j = 1, \dots, N$, and $p, q \in \{-1, 1\}$ in quantum formalism.

11. The inter-connection links are updated using the rotation gate as follows.

$$\varphi[\iota+1][l][l-1][i][j] = \begin{bmatrix} \cos(\frac{\pi}{2}\alpha) & -\sin(\frac{\pi}{2}\alpha) \\ \sin(\frac{\pi}{2}\alpha) & \cos(\frac{\pi}{2}\alpha) \end{bmatrix} \times \varphi[\iota][l][l-1][i][j]$$

where, the inter-linked weight between two successive layers l and $l-1$ at a particular iteration (ι) is $\varphi[\iota][l][l-1][i][j]$ for $l = 1, 2, 3, i = 1, \dots, M, j = 1, \dots, N$

12. The network output is computed as

$$\begin{aligned} \psi[l-1][i][j] = & \sum_{p=-1}^1 \sum_{q=-1}^1 [f_{QMSig}(\psi[l][i+p][j+q] * \varphi[\iota][l][l-1] \\ & \times [i+p][j+q])], \forall l = 2, 3, i = 1, \dots, M, \\ & \times j = 1, \dots, N \end{aligned}$$

13. The network converges until $((\varphi[\iota+1][l][l+1][i][j] - \varphi[\iota][l][l+1][i][j]) < \epsilon_0)$ where ϵ_0 is the permissible error.

14. End

Appendix B. Additional results

The segmented output images obtained using the proposed QIS-Net architecture from slice #10 using transition level ($L = 4, 5, 6, 7$) with four different thresholding activation schemes have been demonstrated in Figs. B.14–B.17. Performance of the proposed QIS-Net architecture for various μ values are demonstrated in Fig. B.18. The empirical cumulative distribution function (ECDF) and standard normal cumulative distribution function (SNCDF) of Dice similarity (DSC) of proposed QIS-Net (for threshold(η_ξ)) and FCNN-4, FCNN-2, U-Net and fuzzy-C-means clustering for all four sets $\{f_1, f_2, f_3, f_4\}$ are presented in Fig. B.19 and Fig. B.20.

References

- [1] V. Gandhi, G. Prasad, D. Coyle, L. Behera, T.M. McGinnity, Quantum neural network-based EEG filtering for a brain-computer interface, *IEEE Trans. Neural Netw. Learn. Syst.* 25 (2) (2014) 278–288.
- [2] C. Chen, D. Dong, H.X. Li, J. Chu, T.J. Tarn, Fidelity-based probabilistic Q-learning for control of quantum systems, *IEEE Trans. Neural Netw. Learn. Syst.* 25 (5) (2014) 920–933.
- [3] P. Li, H. Xiao, F. Shang, X. Tong, X. Li, M. Cao, A hybrid quantum-inspired neural networks with sequence inputs, *Neurocomputing* 117 (2013) 81–90.
- [4] T.C. Lu, G.R. Yu, J.C. Juang, Quantum-based algorithm for optimizing artificial neural networks, *IEEE Trans. Neural Netw. Learn. Syst.* 24 (8) (2013) 1266–1278.
- [5] S. Bhattacharyya, P. Pal, S. Bhowmick, Binary image denoising using a quantum multilayer self organizing neural network, *Appl. Soft Comput.* 24 (2014) 717–729.
- [6] N. Kouda, N. Matsui, H. Nishimura, Image compression by layered quantum neural networks, *Neural Process. Lett.* 16 (1) (2002) 67–80.
- [7] N. Kouda, N. Matsui, H. Nishimura, An examination of qbit neural network in controlling an inverted pendulum, *Neural Process. Lett.* 22 (3) (2005) 277–290.
- [8] K. Takahashi, M. Kurokawa, M. Hashimoto, Multi-layer quantum neural network controller trained by real-coded genetic algorithm, *Neurocomputing* 134 (2014) 159–164.
- [9] D. Konar, S. Bhattacharya, B.K. Panigrahi, K. Nakamatsu, A quantum bi-directional self-organizing neural network (QBDSONN) architecture for binary object extraction from a noisy perspective, *Appl. Soft Comput.* 46 (2016) 731–752.
- [10] D. Konar, S. Bhattacharya, N. Das, B.K. Panigrahi, A Quantum Bi-Directional Self-Organizing Neural Network (QBDSONN) for binary image denoising, in: Proc. IEEE International Conference on Advances in Computing, Communications and Informatics, ICACCI, 2015, 2015, pp. 1225–1230.
- [11] D. Konar, S. Bhattacharyya, B.K. Panigrahi, QIBDS Net: A Quantum-Inspired Bi-Directional Self-supervised Neural Network Architecture for Automatic Brain MR Image Segmentation, in: Proc. 8th International Conference on Pattern Recognition and Machine Intelligence, PReMI 2019, in: Lecture Notes in Computer Science, vol. 11942, 2019, pp. 87–95.
- [12] K.M. Schmainda, M.A. Prah, J.M. Connelly, S.D. Rand, Glioma DSC-MRI perfusion data with standard imaging and ROIs, *Cancer Imaging Arch.* (2019) <http://dx.doi.org/10.7937/K9/TCIA.2016.5D184js8>.
- [13] P. Georgiannis, D. Cavouras, I. Kalatzis, A. Daskalakis, G.C. Kagadis, M. Mala-mas, G. Nikiforidis, E. Solomou, Non-linear least square feature transformations for improving the performance of probabilistic neural networks in classifying human brain tumors on MRI, *Comput. Sci. Appl.-ICCSA* (2007) 239–247.
- [14] V. Kumar, J. Sachdeva, I. Gupta, N. Khandelwal, C.K. Ahuja, Classification of brain tumors using PCA-ANN, in: Proc. of World Congress on Information and Communication Technologies, WICT, 2011, pp. 1079–1083.
- [15] D. Zikic, B. Glocker, E. Konukoglu, J. Shotton, A. Criminisi, D.H. Ye, C. Demiralp, O.M. Thomas, T. Das, R. Jena, S.J. Price, Contextsensitive classification forests for segmentation of brain tumor tissues, in: Med. Image Comput. Comput.-Assisted Intervention Conf.-Brdin Tumor Segmentation Challenge, Nice, France, 2012.
- [16] S. Bauer, T. Fejes, J. Siotboom, R. Wiest, L.P. Nolte, M. Reyes, Segmentation of brain tumor images based on integrated hierarchical classification and regularization, in: Med. Image Comput. Comput.-Assisted Intervention Conf.-Brain Tumor Segmentation Challenge, Nice, France, 2012.
- [17] H. Huang, F. Meng, S. Zhou, F. Jiang, G. Manogaran, Brain image segmentation based on FCM clustering algorithm and rough set, special section on new trends in brain signal processing and analysis, *IEEE Access* (2019) <http://dx.doi.org/10.1109/ACCESS.2019.2893063>.
- [18] A. Ortiz, J.M. Gorri, J. Ramirez, D.S. Gonzalez, MRI Brain image segmentation with supervised SOM and probability-based clustering method, new challenges on bio-inspired applications, in: IWINAC 2011, in: Lecture Notes in Computer Science, vol. 6687, Springer, Berlin, Heidelberg, 2011.
- [19] S. Pereira, A. Pinto, V. Alves, C.A. Silva, Brain tumor segmentation using convolutional neural networks in MRI images, *IEEE Trans. Med. Imaging* 35 (5) (2016).
- [20] Y. Wang, Z. Sun, C. Liu, W. Peng, J. Zhang, MRI Image Segmentation by Fully Convolutional Networks, in: Proc. of 2016 International Conference on Mechatronics and Automation, China, 2016, pp. 1697–1702.
- [21] D. Zikic, et al., Segmentation of brain tumor tissues with convolutional neural networks, in: MICCAI Multimodal Brain Tumor Segmentation Challenge, BraTS, 2014, pp. 36–39.
- [22] M. Lyksborg, et al., An ensemble of 2d convolutional neural networks for tumor segmentation, in: Image Analysis, Springer, New York, 2015, pp. 201–211.
- [23] O. Ronneberger, P. Fischer, T. Brox, U-net: Convolutional networks for biomedical image segmentation, in: International Conference on Medical Image Computing and Computer-Assisted Intervention, Springer, 2015, pp. 234–241.
- [24] G. Wang, Interactive medical image segmentation using deep learning with image-specific fine tuning, *IEEE Trans. Med. Imaging* 37 (7) (2018).
- [25] X. Zhuang, Y. Li, Y. Hu, K. Ma, Y. Yang, Y. Zheng, Self-supervised Feature Learning for 3D Medical Images by Playing a Rubik's Cube, in: International Conference on Medical Image Computing and Computer-Assisted Intervention, MICCAI 2019, 2019, pp. 420–428.
- [26] S. Kak, On quantum neural computing, *Inform. Sci.* 83 (1995) 143–160.
- [27] G. Purushothaman, N.B. Karayiannis, Quantum neural networks (QNNs): inherently fuzzy feedforward neural networks, *IEEE Trans. Neural Netw.* (8) (1997).
- [28] C.Y. Liu, C. Chen, C.T. Chang, L.M. Shih, Single-hidden-layer feed-forward quantum neural network based on grover learning, *Neural Netw.* 45 (2013) 144–150.
- [29] Y. Li, X. Wu, Harmonic Measuring Approach Based on Quantum Neural Network, In Proc. 2012 International Conference on Applied Physics and Industrial Engineering, Physics Procedia, Vol. 24, 2012, pp. 337 – 344.
- [30] N. Matsui, M. Takai, H. Nishimura, A network model based on qbitlike neuron corresponding to quantum circuit, *Electron. Commun. Japan* 3 83 (10) (2000) 67–73.
- [31] S. Miroslav, Wave probabilities and quantum entanglement, *Neural Netw. World: Int. J. Neural Mass - Parallel Comput. Inf. Syst.* 18 (5) (2008) 401–406.
- [32] Nam-H. Nguyen, E.C. Behrman, A. Moustafa, J.E. Steck, Benchmarking neural networks for quantum computations, *IEEE Trans. Neural Netw. Learn. Syst.* (2019) 1–10, <http://dx.doi.org/10.1109/TNNLS.2019.2933394>.
- [33] A. Ghosh, N.R. Pal, S.K. Pal, Self organization for object extraction using a multilayer neural network and fuzziness measures, *IEEE Trans. Fuzzy Syst.* 1 (1) (1993) 54–68.
- [34] D. Konar, S. Bhattacharyya, S. Dey, B.K. Panigrahi, Opti-QIBDS Net: A Quantum-Inspired Optimized Bi-Directional Self-supervised Neural Network Architecture for Automatic Brain MR Image Segmentation, in: Proc. 2019 IEEE Region 10 Conference, TENCON, 2019, pp. 761–766.

- [35] A. Ghosh, Use of fuzziness measures in layered networks for object extraction: a generalization, *Fuzzy Sets and Systems* 72 (3) (1995) 331–348.
- [36] D. Ventura, T. Martinez, An artificial neuron with quantum mechanical properties, in: Proc. Intl. Conf. Artificial Neural Networks and Genetic Algorithms, 1997, pp. 482–485.
- [37] D. McMohan, *Quantum Computing Explained*, John Wiley & Sons, Inc, Hoboken, New Jersey, 2008.
- [38] R.P. Feynman, R.B. Leighton, M. Sands, *The Feynman Lectures on Physics*, Vol. 3, Addison-Wesley Publishing Company, Massachusetts, 1965.
- [39] M.A. Nielson, I.L. Chung, *Quantum Computation and Quantum Information*, Cambridge University press, 2000.
- [40] S. Bhattacharyya, P. Dutta, U. Maulik, Multilevel image segmentation with adaptive image context based thresholding, *Appl. Soft Comput.* 11 (1) (2011) 946–962.
- [41] P. Dutta, *Performance Analysis of Evolutionary Algorithm*, Lambert Academic Publishers, ISBN: 978-3-659-18349-2, 2012.
- [42] M.H. Gail, S.B. Green, Critical values for the one-sided two-sample Kolmogorov–Smirnov statistic, *J. Amer. Statist. Assoc.* 71 (1976) 757–760.